

1 Dynamics of environmental conditions during a decline of a *Cymodocea nodosa* meadow

2

3 Mirjana Najdek¹, Marino Korlević¹, Paolo Paliaga², Marsej Markovski¹, Ingrid Ivančić¹,

4 Ljiljana Iveša¹, Igor Felja³ and Gerhard J. Herndl^{4,5}

5 ¹Center for Marine Research, Ruđer Bošković Institute, G. Paliaga 5, 52210 Rovinj, Croatia

6 ²Department of Natural and Health Sciences, University of Pula, Zagrebačka 30, 52100 Pula,
7 Croatia

8 ³Department of Geology, Faculty of Science, University of Zagreb, Horvatovac 102a, 10000
9 Zagreb, Croatia

10 ⁴Limnology and Bio-Oceanography, Center of Functional Ecology, University of Vienna,
11 Althanstrasse 14, 1090 Vienna, Austria

12 ⁵NIOZ, Department of Marine Microbiology and Biogeochemistry, Royal Netherlands
13 Institute for Sea Research, Utrecht University, PO Box 59, Alberta, Den Burg, 1790, The
14 Netherlands

15 *Correspondence to:* Mirjana Najdek (najdek@cim.irb.hr)

16 **Abstract.** The dynamics of the physicochemical and biological parameters were followed
17 during the decline of a *Cymodocea nodosa* meadow in the northern Adriatic Sea from July
18 2017 to October 2018. During the regular growth of *C. nodosa* from July 2017 to March
19 2018, *C. nodosa* successfully adapted to the changes of environmental conditions and
20 prevented H₂S accumulation by its re-oxidation, supplying the sediment with O₂ from the
21 water column and/or leaf photosynthesis. The *C. nodosa* decline was most likely triggered in
22 April 2018 when light availability to the plant was drastically reduced due to increased
23 seawater turbidity that resulted from increased terrigenous input, indicated by a decrease in
24 salinity accompanied with a substantial increase of particulate matter concentration, combined
25 with resuspension of sediment and elevated autotrophic biomass. Light reduction impaired
26 photosynthesis of *C. nodosa* and the oxidation capability of below-ground tissue.
27 Simultaneously, a depletion of oxygen due to intense oxidation of H₂S occurred in the
28 sediment, thus creating anoxic conditions in most of the rooted areas. These linked negative
29 effects on the plant performance caused an accumulation of H₂S in the sediments of the *C.*
30 *nodosa* meadow. During the decay of above- and below-ground tissues, culminating in
31 August 2018, high concentrations of H₂S were reached and accumulated in the sediment as
32 well as in bottom waters. The influx of oxygenated waters in September 2018 led to the re-
33 establishment of H₂S oxidation in the sediment and remaining of the below-ground tissue.
34 Our results indicate that if disturbance of environmental conditions, particularly those
35 compromising the light availability, takes place during the recruitment phase of plant growth
36 when metabolic needs are at maximum and stored reserves minimal, a sudden and drastic
37 decline of the seagrass meadow occurs.

38

39 **1 Introduction**

40 Seagrasses are important ecosystem engineers constructing valuable coastal habitats which
41 play a key role in the preservation of marine biodiversity and carbon sequestration (Duarte et
42 al., 2013; Samper-Villareal et al., 2016). Seagrasses extend their active metabolic surfaces
43 (i.e., leaves, rhizomes and roots) into the water column and in the sediment, where root
44 activity might modify the chemical conditions (Marbà and Duarte, 2001). Their canopies and
45 dense meadows are responsible for trapping substantial amounts of sediment particles and
46 organic matter, enhancing water transparency and sediment stability with the dense network
47 formed by the rhizome (Gacia and Duarte, 2001; Hendriks et al., 2008; Widdows et al., 2008).
48 Seagrass rhizospheres store organic matter (Pedersen et al., 1997), promote sulfate reduction
49 (Holmer and Nielsen, 1997), release oxygen (Pedersen et al., 1998) and alter sediment redox
50 potential.

51 Seagrasses require some of the highest light levels of any plant worldwide to provide
52 oxygen to roots and rhizomes and support a large amount of non-photosynthetic tissue (Orth
53 et al., 2006). This make seagrasses sensitive to environmental changes, especially those that
54 deteriorate light availability, such as sediment loading, eutrophication or epiphyte cover on
55 seagrass leaves (Terrados et al., 1998; Halun et al., 2002; Brodersen et al., 2015; Costa et al.,
56 2015). Seagrasses have adapted to a highly variable light environment providing tolerance to
57 short-term periods of low light conditions by balancing carbon supply and respiratory
58 requirements. In a healthy growing population this balance is achieved by increasing the
59 photosynthetic activity, re-allocation of carbohydrate reserves from rhizomes and slowing
60 down growth rates (Collier et al., 2009). Beside metabolic and physiological changes, stress
61 responses under poor light conditions include shedding of leaves and shoots and production of
62 new, altered tissue. At sub-lethal light levels, these changes may be permanent. Below these
63 species-specific minimum light requirements seagrass populations are dying off (Collier et al.,
64 2012). Membrane lipids, particularly polyunsaturated fatty acids (PUFA), as the most
65 responsive constituents have a major role in the adaptation processes of primary producers to
66 fluctuating environmental factors, such as temperature, irradiance or salinity (Viso et al.,
67 1993; Lee et al., 2007; Schmid et al., 2014; Sousa et al., 2017; Beca-Carretero et al., 2018;
68 Beca-Carretero et al., 2019). The changes in the unsaturation degree (UND) of membrane
69 fatty acids affect the maintenance of membrane functions and its resistance to cold stress or

70 poor light conditions. UND depends mostly on the variation of α -linolenic (C18:3n-3, ALA)
71 and linoleic (C18:2n-6, LA), the major unsaturated fatty acids in leaves, implicated in the
72 evolution of oxygen during photosynthesis. LA and ALA are derived from oleic acid by
73 desaturation in the chloroplast and this conversion considerably declines in the dark, being
74 completely inhibited by anaerobiosis (Harris and James, 1965).

75 Sediments inhabited by seagrasses are usually anoxic, highly reduced and rich in sulfide
76 (H_2S), a strong phytotoxin (Koch and Erskine, 2001) which has been implicated in several
77 die-off events of seagrasses (Carlson et al., 1994; Borum et al., 2005; Krause-Jensen et al.,
78 2011). H_2S is produced by sulfate-reducing bacteria that use sulfate as a terminal electron
79 acceptor for the mineralization of organic matter (Jørgensen, 1977; Capone and Kiene, 1988,
80 Canfield et al., 1993). High H_2S concentrations may occur as a consequence of enhanced
81 mineralization due to increased temperature, organic loading or oxygen depletion (Moeslund
82 et al., 1994; Pérez et al., 2007; Mascaró et al., 2009). Under these conditions, sulfides may
83 intrude into plant. Re-oxidation of H_2S in the rhizosphere by incorporation of S^0 in the below-
84 ground tissue has been recognized as a major survival strategy of seagrasses in sulfidic
85 sediments (Pedersen et al., 2004; Holmer et al., 2005; Hasler-Sheetal and Holmer, 2015).
86 Generally, the synergistic effect of oxygen depletion and other stresses, such as sulfide
87 toxicity may shorten the survival of benthic communities and possibly accelerate mortality
88 events (Vaquer-Sunyer and Duarte, 2010).

89 The seagrass *Cymodocea nodosa* (Ucria) Ascherson is widely distributed and common
90 species throughout the Mediterranean (Terrados and Ros 1992; Pedersen et al., 1997;
91 Cancemi et al., 2002; Agostini et al., 2003). For the northern Adriatic, however, only sparse
92 data are available on the standing crop, seasonal dynamics or natural/anthropogenic pressures
93 supporting the ecological or conservation status of *C. nodosa* meadows (Zavodnik et al.,
94 1998; Orlando-Bonaca et al., 2015; 2016). Although *C. nodosa* show large phenotypic
95 plasticity adapting to diverse natural and anthropogenic stressors by physiological and
96 morphological adaptations, a severe decline has been reported during the last decades in
97 coastal areas (Orth et al., 2006; Short et al., 2011; Tuya et al., 2002; 2014), including the
98 northern Adriatic (Orlando-Bonaca et al., 2015; 2019). One of these declines was documented
99 in our study performed from July 2017 to October 2018 in Saline Bay (northern Adriatic Sea).
100 A series of monthly physicochemical and biological measurements were conducted in *C.*
101 *nodosa* tissues, sediment underlying the *C. nodosa* meadow, non-vegetated sediments and

102 surrounding water to i) determine the link between ambient seawater and sediment
103 environmental factors influencing the growth of *C. nodosa*, ii) document the response of *C.*
104 *nodosa* to the changes in environmental conditions that led to the meadow decline and iii)
105 evaluate the conditions leading to the decline of *C. nodosa*.

106 **2 Materials and methods**

107 2.1 Study site

108 Saline Bay is located 4 km northwest of Rovinj (Croatia) at the coast of the northern Adriatic
109 Sea (45°7'5"N; 13°37'20"E, Fig. S1). The bay represents the terminal shallow part of an 800
110 m long inlet, open towards the northwest. The southeastern coast of Saline Bay is
111 characterized by relatively pristine conditions, while the northwestern littoral part has been
112 completely modified by the excavation of coastal mud and the addition of large amounts of
113 gravel to create an artificial beach. Large amounts of silty red soil (*terra rossa*) can be found
114 in the south eastern inner part of the bay in a large muddy flatland which is slowly being
115 eroded by the sea and rain weathering. The main input of freshwater to the bay represents land
116 drainage canals since the year 2017. Even though Saline Bay is protected from the prevailing
117 winds (from the NE and SE) circulations from the northwestern quadrant can occasionally
118 trigger bigger waves resuspending the surface sediments and giving the waters a muddy
119 appearance. At the beginning of this study, the seafloor was covered with large *C. nodosa*
120 meadows spreading from the southwestern coastal area (1.5 m depth) toward the central part
121 of the bay (4 m depth), while at the end of the study only a few small patches persisted in tiny
122 stripes along the shoreline.

123

124 2.2 Sampling

125 The sampling was performed for 15 months from July 2017 to October 2018. Seawater for
126 analyses of nutrients, chlorophyll *a* (Chl *a*), particulate matter concentration and prokaryotic
127 abundance was sampled using plastic containers (10 L). *C. nodosa* (3 – 4 m of depth) was
128 collected together with rhizomes, roots and epiphytic macroalgae by divers using the quadrat
129 sampling method. Three quadrats (20 x 20 cm) were randomly scattered in positions of
130 maximum seagrass coverage (e.g. 100 %). Sediment samples were collected inside vegetated
131 and non-vegetated sediment by divers using plastic core samplers (15 cm, 15.9 cm²). For
132 granulometric composition, organic matter, prokaryotic abundance, total lipids and fatty acid
133 analyses, the cores were cut into 1 cm sections to a depth of 8 cm and lyophilized, except of

134 sections for prokaryotic abundance analysis, that were weighted (approx. 2 g) and fixed with
135 formaldehyde (final conc. 4% v/v) immediately after slicing the sediment core.

136

137 2.3 Temperature (T) and salinity (S) measurements

138 T was measured continuously (in 30 min. intervals) using HOBO pendant temp/light Data
139 Loggers (Onset, USA) which were replaced at each sampling. S was measured on sampling
140 dates by a pIONneer 65 probe (Radiometer analytical, Copenhagen).

141

142 2.4 Inorganic nutrients, Chl *a* and particulate matter (PM) analysis

143 Seawater for all analysis was filtered through combusted Whatman GF/F filters. Nitrate
144 (NO₃), nitrite (NO₂), ammonia (NH₄), phosphate (PO₄) and silicate (SiO₄) were analyzed
145 spectrophotometrically according to Strickland and Parsons (1972). Chl *a* was determined on
146 filters by the fluorometric procedure after extraction in 90 % acetone (Holm-Hansen et al.,
147 1965). PM was determined gravimetrically after filtering up to 5L seawater on pre-weighed,
148 filters which were dried (at 60°C) and reweighed.

149

150 2.5 Determining prokaryotic abundance

151 For determining the prokaryotic abundance in seawater, 2 ml of formaldehyde (final conc. 4%
152 v/v) fixed samples were stained with 4,6-diamidino-2-phenylindol (DAPI, 1 µg mL⁻¹ final
153 conc.) for 10 min (Porter and Feig, 1980). In sediment samples, prokaryotes were detached
154 from the sediment particles by addition of Tween 80 (0.05 mL) and ultrasonicated for 15 min
155 (Epstein and Rossel, 1995). After sonication, 1 mL of the supernatant was stained with DAPI
156 (final conc. 5 µg/mL). DAPI stained samples were filtered onto black polycarbonate filters
157 (Whatman, Nuclepore, 0.22 µm) and counted under an epifluorescence microscope (Zeiss
158 Axio Imager Z1).

159

160 2.6 Biometry of *C. nodosa* and epiphytic macroalgae

161 The material from each quadrat was washed under running seawater to remove sediment.
162 From each quadrat algae, leaves and rhizomes with roots were separated. The length of the
163 longest leaf on each shoot was measured and the shoots were counted. Species of macroalgae
164 were determined, and their coverage was estimated according to the Braun-Blanquet scale.

165 Separated samples were washed with filtered and autoclaved seawater, weighed, dried at 60
166 °C for 48 h and re-weighed. The dry mass was calculated per area (g m^{-2}).

167

168 2.7 Granulometric composition of the sediment and its organic matter content

169 For granulometric analysis of the sediment, each sample was wet sieved through a set of
170 seven standard ASTM sieves (4-, 2-, 1-, 0.5-, 0.25-, 0.125-, 0.063-mm mesh size). The
171 fraction that passed through the 0.063-mm sieve was collected and analyzed following the
172 standard sedigraph procedure (Micromeritics, 2002). The material that was retained on the
173 sieves was dried and weighted. The data obtained by both techniques were merged to obtain a
174 continuous grain size range and analyzed with the statistic package Gradistat v 6.0. Sediments
175 were classified according to Folk (1954). The sediment permeability was calculated based on
176 median grain size (d_g) following the empirical relation by Gangi (1985). The organic matter
177 content was determined as ignition loss after heating dried sediment sections at 450°C for 4 h
178 in a muffle furnace.

179

180 2.8 Oxygen (O_2), hydrogen sulfide (H_2S) and redox potential (Eh) profiling

181 The microprofiles of O_2 , H_2S and Eh were measured on intact cores immediately after
182 sampling using a motorized micromanipulator (MMS9083) equipped with microsensors OX-
183 100 and H_2S -200, redox microelectrode RD-200 coupled with reference electrode REF-RM
184 (Unisense A/S, Denmark). Prior to the measurements, the OX-100 microsensor was calibrated
185 using a two-point oxic – anoxic calibration; H_2S -200 was calibrated in fresh Na_2S solutions
186 using eight-point calibration ($1\mu\text{M}$ - $300\mu\text{M}$ in a de-oxygenated calibration buffer
187 (NaAc/HAc , $\text{pH} < 4$); RD-200 with REF-RM was calibrated using two point calibration by
188 simultaneous immersion of electrodes in quinhydrone redox buffers prepared in pH 4 and pH
189 7 buffers, all according to the manufacturer's recommendation. During measurements,
190 sediment cores were placed in a pool filled with seawater from the sampling site to maintain
191 *in situ* temperature. From July to October 2017 H_2S was measured spectrophotometrically in
192 pore waters (Cline, 1969) squeezed out by centrifugation from each section (5 mm) of the
193 sediment cores.

194

195 2.9 Total lipids, fatty acid composition and elemental sulfur (S^0)

196 Lyophilized samples of seagrass tissues, macroalgae, sediment or particulate matter were
197 weighed and extracted into a solvent mixture of dichloromethane/methanol (DCM: MeOH,
198 2:1) in an ultrasonic bath at 35°C with three solvent mixture changes. The extracts were
199 pooled and separated into layers by addition of 0.9% NaCl solution. Lower DCM layers
200 (containing lipids) were released over Na₂SO₄ anhydride, collected in pre-weighed round
201 bottom flasks and evaporated to dryness using rotavapor. After evaporation, flasks were re-
202 weighed, and total lipid concentrations (TL, mg g⁻¹ DW) were calculated from the difference
203 in weight. For fatty acids determination, lipid extracts were saponified (1.2 M NaOH in
204 methanol), acidified (6 M HCl), methylated (14% BF₃ in methanol) and extracted into DCM.

205 Fatty acid methyl esters (FAME) were analyzed by Agilent gas-liquid chromatography
206 (GLC) 6890 N GC System equipped with a 5973 Network Mass Selective Detector, capillary
207 column (30 m x 0.3 mm x 0.25 μm; cross-linked 5 % phenylmethylsiloxane) and ultra-high
208 purity helium as the carrier gas. The GLC settings were as follows: programmed column
209 temperature rise from 145°C by 4°C/min to 215°C, then by 1°C/min to 225°C and finally by
210 4°C/min to 270°C at constant column pressure of 2.17 kPa. Retention times, peak areas and
211 mass spectra were recorded on the ChemStation Software. FAME were identified by mass
212 spectral data and family plots of an equivalent chain length (ECL) for GC standards. Applied
213 GC standards were: FAME mix C18–C20, PUFA1, PUFA3 standards (Supelco/Sigma-
214 Aldrich, Bellefonte, PA, USA); C4–C24 FAME standard mix, cod liver oil and various
215 individual pure standards (Sigma, Neustadt, Germany).

216 The following indices of fatty acid profiles were calculated: saturated fatty acids (SAT),
217 monounsaturated fatty acids (MUFA), polyunsaturated fatty acids (PUFA) and the
218 unsaturation degree (UND). UND was employed to evaluate the degree of organic matter
219 degradation due to more susceptibility of unsaturated, particularly polyunsaturated,
220 components to degradation and calculated according to the formula
221 $[1*(\% \text{ mono-})+2*(\% \text{ di-})+3*(\% \text{ tri-})+4*(\% \text{ tetra-})+5*(\% \text{ penta-})+6*(\% \text{ hexa-enoic})]/\% \text{ SAT}$
222 (Pirini et al., 2007). To evaluate the input of terrestrial organic matter relative to that of
223 marine origin in particulate matter, the terrestrial to aquatic acid ratio (TAR= C24+C26+C28 /
224 C12+C14+C16) was used (Cranwell et al., 1987; Bourbonniere and Meyers, 1996).

225 In FAME chromatograms elemental sulfur (S⁰), eluted as S₈ (m/z 256), was identified by
226 comparison of retention time and characteristic fragment ions in samples and standard
227 solutions. The concentration of S⁰ was estimated on the base of the calibration curve prepared

228 for standard solution of S₈ (Aldrich, Germany) in cyclohexane (2-20 mg L⁻¹). The calibration
229 curve was determined under the same GLC settings as FAME. Limit of detection (LoD) and
230 limit of quantitation (LoQ) were calculated from the parameters of the calibration curve
231 constructed on the basis of the 3 lowest concentrations in 3 replicates. LoD and LoQ (0.92 mg
232 L⁻¹ and 2.80 mg L⁻¹, respectively) were more than twice the values obtained by Rogowska et
233 al. (2016) probably due to higher injector and column temperature used in this study than they
234 proposed as optimal for S determination.

235

236 2.10 Data analyses

237 A multivariate analysis, hierarchical clustering and K-means methods (Systat 12) was applied
238 to group *C. nodosa* above- and below-ground tissues according to the similarity of their fatty
239 acid profiles and indices, i.e., physiological condition during the investigated period.

240 Sediment data were analyzed for two groups of sediment layers, the upper layer (0- 4 cm)
241 where most of rhizomes and roots are located, and the lower layers (5-7 cm). Differences
242 between vegetated and non-vegetated sediment samples in each sediment layer were tested by
243 one-way ANOVA. Correlations among parameters were tested using the Pearson's correlation
244 coefficient (r). The level of statistical significance was $p < 0.05$. A multivariate principal
245 component analysis (PCA, Primer 6) was applied to identify the most important variables
246 explaining differences between vegetated and non-vegetated sediments. Correlation matrices
247 were constructed using variables: H₂S, Eh, O₂, S⁰, PA, TL and UND. All variables were
248 normalized due to their different scales. Only the principal components with eigenvalues >1
249 were considered.

250

251 **3 Results**

252 3.1 Water column

253 3.1.1 Environmental variables

254 During summer of 2017 daily means of sea-bottom temperature in *C. nodosa* meadow ranged
255 between 26°C and 28°C. During autumn seawater temperatures decreased below 12°C until
256 the end of December. The coldest period was recorded at the beginning of March lasting only
257 for a few days (min. 8.62°C). From April to mid-July 2018, temperature increased with
258 moderate fluctuations to the maximum of 29.26°C recorded in August 2018 (Fig. 1a).

259 Concentrations of inorganic nutrients and Chl *a* were generally low. The highest
260 concentrations (DIN: 8.27 μM ; PO_4 : 0.18 μM ; SiO_4 : 9.82 μM ; Chl *a*: 0.89 $\mu\text{g L}^{-1}$) associated
261 with the lowest salinity (34.2) were found in September 2017 (Table S1). The abundance of
262 prokaryotes ($2.6\text{-}11.3 \times 10^5 \text{ cell mL}^{-1}$) varied seasonally and significantly correlated to
263 seawater temperatures ($r = 0.618$; $p < 0.05$). In contrast, salinity (S: 34.2 - 38.5) and
264 concentrations of particulate matter (PM: 3.84 - 14.21 mg L^{-1}) showed irregular variations
265 (Fig. 1b) and a significant opposite trend ($r = -0.630$; $p < 0.05$).

266 The particulate lipids exhibited the highest unsaturation degree (UND) during
267 summer/early autumn 2017 and small increases of UND in April and September/October
268 2018 (Fig. 1c). UND was significantly correlated with Chl *a* ($r = 0.603$; $p < 0.05$). In contrast,
269 terrestrial to aquatic ratio (TAR) considerably increased in April and was the highest in
270 August 2018 (Fig. 1c). TAR was negatively correlated to UND ($r = -0.644$, $p < 0.05$) and
271 positively to particulate matter ($r = 0.641$, $p < 0.05$). Although PUFA with 18 C atoms made
272 the largest contribution to the total PUFA pool, C20 PUFA, mainly of phytoplankton origin,
273 showed a similar trend as observed for UND (Fig. S2, Table S2).

274

275 3.2 *Cymodocea nodosa* meadow

276 3.2.1 Biometry

277 *C. nodosa* leaves and shoots reached the highest biomass ($285.3 \pm 57.4 \text{ g m}^{-2}$), length ($102.4 \pm$
278 26.6 mm) and shoot density ($3703 \pm 334 \text{ shoots m}^{-2}$) in October 2017 (Fig. 2a). After the
279 appearance of the regular vegetation minimum in November 2017, biometric indices further
280 decreased reflecting the decay of the meadow in summer 2018. In August 2018, only yellow
281 to brownish leaves on sparse shoots were collected ($4.5 \pm 1.3 \text{ g m}^{-2}$, $5.4 \pm 1.3 \text{ mm}$ and 30 ± 35
282 shoots m^{-2}). In September and October 2018, no shoots or leaves were observed (Fig. 2a). The
283 biomass of rhizomes and roots reached also its maximum in October 2017 ($599.7 \pm 36.8 \text{ g m}^{-2}$).
284 In contrast to leaves and shoots, the below-ground biomass was stable until March 2018
285 when a decline was observed that continued until October 2018 ($30.5 \pm 6.8 \text{ g m}^{-2}$) (Fig. 2a).

286

287 3.2.2 Total lipid (TL) concentrations and fatty acid composition

288 TL in the *C. nodosa* above-ground tissue ($6.7 - 25.3 \pm 2.4 \text{ mg g}^{-1} \text{ DW}$) increased until
289 February 2018, when maximum TL concentrations were measured (Fig. 2b). Thereafter, TL
290 concentrations decreased until August 2018. During this period, the below-ground TL

291 concentration ($6.3 \pm 1.9 - 15.9 \pm 1.1 \text{ mg g}^{-1} \text{ DW}$) was generally lower than the above-ground
292 TL concentrations and the trend was similar to that of leaves. The minimum concentrations of
293 TL were observed in September 2018, while in October 2018, concentrations similar to that
294 measured in October 2017 were observed (Fig. 2b).

295 The major fatty acid components in *C. nodosa* tissues were palmitic (C16:0) amongst the
296 saturated (SAT) and oleic (C18:1n-9) in monounsaturated fatty acids (MUFA). In the above-
297 ground tissue, the main polyunsaturated fatty acids (PUFA) were α -linolenic (C18:3 n-3,
298 ALA) and linoleic (C18:2 n-6, LA), while in the below-ground tissue LA was dominant (Fig.
299 2b). The dynamics of UND in the above-ground tissue was principally influenced by changes
300 in ALA and LA. LA/ALA ratios were < 1 from July 2017 to March 2018, and > 1 from April
301 to July 2018 (Fig. 2b). In August 2018, the LA/ALA ratio was infinite due to the absence of
302 ALA (Fig. 2b). Elemental sulfur (S^0) was detected only in decaying leaves in August 2018
303 ($0.21 \text{ mg g}^{-1} \text{ DW}$). In the below-ground tissue, S^0 was detected in all samples (Fig. 2b).
304 Higher concentrations were measured during summer 2017 (up to $0.39 \pm 0.06 \text{ mg g}^{-1} \text{ DW}$). S^0
305 increased from minimum concentrations in April ($0.02 \pm 0.01 \text{ mg g}^{-1} \text{ DW}$) until September
306 2018 reaching $1.42 \text{ mg g}^{-1} \text{ DW}$ (Fig. 2b).

307 According to the fatty acid profiles, *C. nodosa* leaves were classified in three groups,
308 except for the leaves collected in August 2018 (Fig. 3). The most distinguishing features
309 specifying physiological differences between Group 1 (July - October 2017 and February -
310 March 2018), Group 2 (November - December 2017 and April - May 2018) and Group 3
311 (June and July 2018) were decreasing mean values of PUFA, UND, ALA and LA and
312 increasing means of SAT and the proportion of long-chain saturated fatty acids ($C \geq 24$). In
313 the ungrouped leaves from August 2018 ALA was not found, PUFA and UND were at a
314 minimum, while SAT and $C \geq 24$ at a maximum (Table S3). Three groups of rhizomes and
315 roots (Group 1: July - October 2017 and February - March 2018; Group 2: November -
316 December 2017 and April - May 2018 and Group 3: (June - October 2018) showed similar
317 characteristics to the groups 1, 2 and 3 of related leaves (Table S4).

318

319 3.2.3 Epiphytic macroalgae

320 From July 2017 to February 2018 different taxa of macroalgae belonging to the three phyla
321 Chlorophyta (*Halimeda tuna*, *Dasycladus vermicularis*, *Cladophora prolifera*, *Udotea*
322 *petiolata*), Rhodophyta (*Rytiphlaea tinctoria*, *Peyssonnelia* spp, *Gelidium* sp.) and

323 Ochrophyta (*Dictyota dichotoma*) were covering the meadow in varying proportions and
324 abundances (Fig. 4). After March 2018, when only few individuals of *Peyssonnelia* sp. were
325 found, macroalgae were no longer present in the *C. nodosa* meadow.

326 Although the fatty acid profiles of macroalgal communities were highly variable, the
327 contribution of 18- and 20 PUFA to the total PUFA pool generally depended on the prevailing
328 phyla and their characteristic PUFA pattern. The algae belonging to Rhodophyta and
329 Ochrophyta are richer in 20 PUFA (C20:5n-3, C20:4n-6), while Chlorophyta are generally
330 showing prevalence of 18 PUFA (C18:3n-3, C18:2n-6) (Schmid et al., 2014, Gao et al.,
331 2018). Furthermore, their contribution to biomass varied due to large differences in
332 morphology, which most likely also contributed to the variability of fatty acid profiles. 18
333 PUFA and 20 PUFA showed the highest contribution to the total PUFA pool during the
334 dominance of Chlorophyta and Rhodophyta in the macroalgal community, respectively. In
335 most samples, the lowest contribution to the total PUFA pool was observed for 16 PUFA and
336 22 PUFA (Fig. S3).

337

338 3.3 Sediment

339 3.3.1 Granulometric composition

340 According to the granulometric composition, median grain sizes (d_g) and permeability (k) the
341 vegetated and non-vegetated sediments were classified as slightly gravelly sandy mud (g)sM,
342 fine grained ($d_g < 165 \mu\text{m}$) and low permeable to impermeable sediment ($k < 2 \cdot 10^{-11} \text{ m}^2$). In
343 general, the *C. nodosa* sediment consisted of a significantly higher proportion of sand (Sa),
344 and lower proportion of silt (Si) and clay (C) (Sa, $41.11 \pm 4.34 \%$; Si, $46.44 \pm 2.86 \%$; C, 9.63
345 $\pm 2.76 \%$) in comparison to non-vegetated sediment (Sa, $20.53 \pm 10.49 \%$; Si, $53.24 \pm 6.76 \%$;
346 C, $23.29 \pm 4.86 \%$). The median grain size and permeability in *C. nodosa* sediment (d_g , 37.51
347 $\pm 17.97 \mu\text{m}$, k , $1.22 \cdot 10^{-12} \pm 1.13 \cdot 10^{-12} \text{ m}^2$) were significantly higher than in non-vegetated
348 sediment (d_g , $10.86 \pm 5.34 \mu\text{m}$; k , $1.04 \cdot 10^{-13} \pm 1.02 \cdot 10^{-13} \text{ m}^2$). The upper layers of both cores
349 (0 - 4 cm) had larger particles, while the lower layers (5 - 8 cm) showed a uniform distribution
350 of smaller grain sizes (Fig. 5).

351

352 3.3.2 O_2 , E_h , H_2S and S^0

353 Oxygen concentrations (O_2) in the bottom water of the *C. nodosa* meadow varied in a wide
354 range ($0 \mu\text{M}$ - $171.4 \pm 17.6 \mu\text{M}$) and generally followed the O_2 saturation trend (Fig. 6a).

355 From May to June 2018, O₂ decreased below 62.5 μM, considered as severe hypoxia (Vaquer-
356 Sunyer and Duarte 2008) and was completely depleted in July 2018 (Fig. 6a). From August to
357 October 2018, O₂ increased again. The variations of O₂ in the bottom water of the non-
358 vegetated sediment were similar to those in the *C. nodosa* meadow albeit generally higher
359 (79.4 ± 10.4 μM – 212.2 ± 33.4 μM) than in the vegetated sediment except for September and
360 October 2018 (Fig. 6a).

361 In general, O₂ penetration depth in the vegetated and non-vegetated sediment co-varied
362 with the O₂ concentration in the bottom layer, penetrating deeper when its concentration in the
363 bottom water was higher (Fig. 6b). In the vegetated sediment, O₂ was mainly depleted down
364 to 1 cm of depth. In the non-vegetated sediment, the oxygen penetration depth was up to 4
365 times higher than in vegetated sediments, except for the period from August 2018 to October
366 2018 when the penetration depths were similar (Fig. 6b).

367 The thickness of the oxic (Eh > 150 mV) and suboxic (150 mV > Eh > 0 mV) layers in the
368 vegetated sediment increased from July 2017 (~ 0.5 cm) to March 2018 (~ 4 cm), and
369 decreased progressively from April (~ 0.8 cm) towards the surface in July 2018, when the
370 entire sediment core was anoxic (Eh < 0). From August (~ 1 cm) to October 2018 (~ 2.5 cm)
371 the oxic and suboxic layer thickness increased again (Fig. 7). Oxic conditions (Eh > 0)
372 generally reflected O₂ concentrations in the bottom waters. The dynamics of Eh in non-
373 vegetated sediment were similar to those in the vegetated sediment. However, the thickness of
374 the oxic layer was considerably larger than in the vegetated sediment. Reducing conditions
375 (Eh < 0) were only recorded in July and August 2017 (Fig. 7).

376 Concentrations of free H₂S in the pore water of the vegetated sediment generally increased
377 with depth creating an accumulation zone mainly within the upper sediment layers (1 - 4 cm)
378 (Fig. 7). From July to November 2017, H₂S concentrations increased up to 120 μM (at 4 - 5
379 cm). In December 2017, H₂S was low and uniformly distributed throughout the core (< 5
380 μM). H₂S concentrations increased and the accumulation layer was ascending from March (up
381 to 34.2 ± 12.8 μM; 5 - 7 cm) to April 2018 (up to 177.2 ± 125.1 μM; 3.5 - 4.5 cm). During
382 May 2018 (up to 107.8 ± 75.9 μM; 2.5 - 4 cm), June (up to 199.0 ± 6.3 μM; 1.5 - 6 cm) and
383 July (up to 210.1 ± 138.9 μM; bottom water - 6 cm) a propagation of the accumulation zone
384 was observed in addition to an increase in H₂S (Fig. 7). In August 2018 (up to 1164.1 ± 702.1
385 μM; bottom water - 7 cm) extremely high concentrations over the entire sediment core were
386 recorded. In September and October 2018, H₂S concentrations decreased (down to 140.0 ±

387 25.3 and $72.7 \pm 52.7 \mu\text{M}$; bottom water - 7 cm and 1 - 7 cm, respectively). In the non-
388 vegetated sediment, H_2S depth profiles were similar to those in vegetated sediments, but the
389 concentrations were generally lower, except for the summer of 2017 when the concentrations
390 were comparable but the accumulation zones deeper (Fig. 7).

391 S^0 mainly occurred in oxic ($\text{Eh} > 150 \text{ mV}$) and suboxic ($150 \text{ mV} > \text{Eh} > 0 \text{ mV}$) layers of
392 both, vegetated and non-vegetated sediments (Fig. 7). Generally, the ranges of approximated
393 S^0 concentrations in vegetated sediment ($8.5 \cdot 10^{-5} - 0.39 \text{ mg} \cdot \text{g}^{-1} \text{ DW} \sim 2.6 \cdot 10^{-3} - 12.1 \mu\text{mol} \cdot \text{g}^{-1}$
394 DW), except for the extreme value in April 2018 ($0.99 \text{ mg} \cdot \text{g}^{-1} \text{ DW} \sim 30.8 \mu\text{mol} \cdot \text{g}^{-1} \text{ DW}$),
395 were similar to those found at the non-vegetated sites ($2.9 \cdot 10^{-4} - 0.28 \text{ mg} \cdot \text{g}^{-1} \text{ DW} \sim 9.2 \cdot 10^{-3} -$
396 $8.9 \mu\text{mol} \cdot \text{g}^{-1} \text{ DW}$).

397

398 3.3.3 Prokaryotic abundance

399 Prokaryotic abundance varied largely in vegetated ($2.1 - 39.9 \cdot 10^7 \text{ cells g}^{-1}$ fresh weight, FW)
400 and non-vegetated sediments ($3.7 - 24.1 \cdot 10^7 \text{ cells g}^{-1}$ FW). Prokaryotic abundance was
401 significantly higher in the upper than the lower layers of vegetated ($F = 40.553, p < 0.05$) and
402 non-vegetated ($F = 52.531, p < 0.05$) sediments (Fig. 8). Prokaryotic abundance showed
403 significant monthly changes in the upper ($F = 3.053, p < 0.05$) and lower layer ($F = 5.035, p <$
404 0.05) of vegetated sediments, in contrast to both layers of non-vegetated sediments ($p > 0.05$).
405 Prokaryotic abundances were significantly higher in the upper layers ($F = 44.577, p < 0.05$)
406 and significantly lower in the lower layers ($F = 5.986, p < 0.05$) of vegetated than in the
407 respective layers of non-vegetated sediments (Fig. 8). In the upper sediment layer, prokaryotic
408 abundances were significantly higher in the vegetated than in the non-vegetated sediments
409 from July to October 2017 and from June to August 2018 (Fig. 8). In the lower layers of
410 vegetated sediments, prokaryotic abundance was significantly higher than in the non-
411 vegetated sediments in October 2017 and in August and September 2018 (Fig. 8).

412

413 3.3.4 Organic matter, total lipids and fatty acid composition

414 The concentrations of organic matter (OM) and total lipids (TL) were highly correlated in
415 vegetated (OM: $37.6 - 231.1 \text{ mg/g DW}$, TL: $0.15 - 2.75 \text{ mg/g DW}$; $F = 214.172, p < 0.05$) as
416 well as in non-vegetated sediments (OM: $56.7 - 160.3 \text{ mg/g DW}$, TL: $0.33 - 2.39 \text{ mg/g DW}$; F
417 $= 45.569, p < 0.05$). OM and TL generally decreased with depth and exhibited similar

418 changes throughout the investigated period with significantly higher concentrations in upper
419 than in lower sediment layers ($p < 0.05$) (Fig. 9).

420 In the vegetated sediment, TL showed significant monthly changes in the upper ($F =$
421 11.418, $p < 0.05$) and lower sediment layers ($F = 3.186$, $p < 0.05$), in contrast to both layers of
422 non-vegetated sediment ($p > 0.05$). From July to October 2017, in the upper layer of vegetated
423 sediments, TL was significantly higher than in non-vegetated sediments (Fig. 9). From
424 November 2017 onwards, TL decreased slightly until April 2018, reaching similar
425 concentrations as TL in non-vegetated sediments (Fig. 9). TL concentrations decreased
426 markedly in May and continued until August 2018. During that period, TL in vegetated
427 sediments was significantly lower than in non-vegetated sediments. In September and October
428 2018, TL concentrations in vegetated sediments were similar to those in non-vegetated
429 sediment (Fig. 9).

430 The fatty acid composition of vegetated and non-vegetated sediments was similar and in
431 both layers characterized by the prevalence of SAT (vegetated upper: 71.2 - 90.4%, lower:
432 75.9-89.1%; non-vegetated upper: 71.2-80.7%, lower: 78.2-82.5%) over MUFA (vegetated
433 upper: 7.6-22.9%, lower: 9.0-19.9%; non-vegetated upper: 17.8-24.1%, lower: 15.3-18.2%)
434 and PUFA (vegetated upper: 1.9-6.9%, lower: 1.9-5.1%; non-vegetated upper: 1.7-4.8%,
435 lower: 1.7-3.9%). The trends of the monthly changes in UND were similar in both layers of
436 both sediment types. Those variations were less pronounced in the non-vegetated sediment
437 where UND varied in narrower ranges in both layers (upper: 0.26-0.51, lower: 0.23-0.33) than
438 in vegetated sediment (upper: 0.13-0.57, lower: 0.14-0.37). From July to October 2017 and in
439 April 2018, UND was higher in the upper layers of vegetated sediment than in non-vegetated
440 one, while from November 2017 to March 2018, UNDS of both sediments were lower than in
441 previous period (Fig. 9). From June to August 2018, UND decreased considerably in
442 vegetated sediment, being lower than in non-vegetated sediments. During September and
443 October 2018, an increase of UND was observed in both sediments. In the lower layers,
444 UNDS were similar, except for July and August 2018 when a considerable decrease of UND
445 was observed in vegetated sediments (Fig. 9).

446 The proportions of PUFAs with chain lengths of 16, 18, 20, and 22 C atoms within the
447 PUFA pool were similar between the respective layers of both sediments. Throughout the
448 study period, the highest contribution of 18PUFA originated from *C. nodosa* detritus and
449 Chlorophyta was observed (Fig. S4, Table S2). From July to October 2017, April to May

450 2018 and September to October 2018, a contribution of 20PUFA attributed to phytoplankton
451 and Rhodophyta was also detected. 16PUFA and 22PUFA accounted for the smallest
452 contribution to the PUFA pool and were found in seston and macroalgae (Fig. S4, Table S2).
453 The similarities between the sediments were also observed in the contribution of the main
454 SAT components to the SAT pool from July 2017 to March 2018 and from September to
455 October 2018 (Fig. S4, Table S2). From April to August 2018, an increase of the long-chain
456 ($C \geq 24$) and common (C16:0 + C18:0) fatty acids followed by the decrease of bacterial fatty
457 acids (BACT) contribution to the SAT pool was observed in both layers of the vegetated
458 sediment. In contrast, the contribution of these components to the SAT pool was fairly
459 invariable in non-vegetated sediments during the same period (Fig. S4, Table S2).

460

461 3.3.5 Relationship between different physicochemical parameters

462 The relationships between H_2S , O_2 , TL, S^0 , PA, Eh and UND in vegetated and non-vegetated
463 sediment are shown in the principal component analysis, where PC1 explained 42.5 % and
464 PC2 14.4 % of variability (Fig. 10). The loadings for positive relationships were obtained for
465 H_2S (0.298) on PC1 and Eh (0.541) and O_2 (0.327) on PC2. For the negative relationships, the
466 loadings were for TL (-0.534), UND (-0.494), S^0 (-0.388), Eh (-0.327), PA (-0.296) and O_2 (-
467 0.191) on PC1, and H_2S (-0.536), S^0 (-0.485), TL (-0.165) and UND (-0.221) on PC2.

468 PC1 separated most of the upper sediment layers (July 2017 - May 2018, September -
469 October 2018) according to the higher concentrations of TL and S^0 , higher UND and more
470 positive Eh from the most of the lower layers and upper layers of vegetated sediments (June -
471 August 2018) with increased H_2S concentrations. On PC2, the vegetated was separated from
472 the non-vegetated sediment due to higher concentrations of H_2S , S^0 and more negative Eh,
473 which characterized vegetated sediments during almost the entire study period. The extreme
474 concentrations of S^0 and H_2S found in the upper layer in April and the lower layer in August
475 2018, respectively, were responsible for the considerable separation of these layers from all
476 other vegetated layers (Fig. 10).

477

478 4 Discussion

479 Saline Bay is a shallow, highly dynamic coastal area characterized by frequent turbid waters
480 due to the combined effect of land run-off and wind-driven resuspension of fine sediment.

481 Nutrients and Chl a (as a proxy for autotrophic biomass) varied in the ranges characteristic for

482 the oligotrophic coastal waters off Rovinj (Ivančić et al., 2018). The dynamics of particulate
483 matter was associated with freshwater input. The higher contribution from autochthonous
484 sources was observed during the increases of autotrophic biomass. However, only in
485 September 2017, this increase was supported by nutrients from the water column, while all
486 other increases were most likely connected to bottom waters where phytoplankton could have
487 been supplied with nutrients through sediment resuspension. The considerable increase in the
488 particulate matter of terrigenous origin from April to August 2018 suggested the enhanced
489 land run-off in that period.

490 In temperate Mediterranean coastal waters *C. nodosa* meadows show a clear unimodal
491 annual growth cycle, reaching maximum development in summer, and minima during winter
492 and a particularly active growth phase in spring (Terrados and Ross, 1992; Zavodnik et al.,
493 1998; Agostini et al., 2003). In Saline Bay, the maximum biomass was measured in October
494 2017. This shift from summer to early autumn was most likely due to an intense grazing
495 activities (Cebrian et al., 1996; Valentine and Duffy, 2006) suggested by a prevalence of
496 visibly grazed leaves during July and August 2017. A minimum growth occurred during late
497 autumn/winter, as commonly observed. However, during the spring 2018, phenological
498 parameters continued to decrease in spite of established favorable environmental conditions
499 for growth, i.e., increase in water temperature, intensity and period of solar radiation. This
500 decrease continued until the complete extinction of the above-ground tissue in August 2018.
501 The below-ground tissue followed a similar trend, but with less expressed changes. Still, their
502 recognizable remnants were found after the loss of the above-ground tissues.

503 Organic matter and closely correlated total lipids in the sediment of *C. nodosa* rooted area
504 changed significantly throughout the investigated period, in contrast to organic matter in non-
505 vegetated sediment. Nevertheless, considerable similarity in the quality and degradation of
506 lipid matter at both, the vegetated and the non-vegetated sites indicates an important
507 contribution of detritus imported from the meadow as a source of organic matter for
508 prokaryotes in non-vegetated sediments. This close coupling could be expected due to site
509 proximity and lower organic content of the non-vegetated sediment, which should enhance the
510 dependence of prokaryotes on the imports of seagrass detritus from the adjacent meadows
511 (Holmer et al., 2004). Significant enrichment of *C. nodosa* sediment with unsaturated, more
512 labile components only during abundant growth of meadow could be explained by more
513 efficient entrapment of seston material within the meadow (Gacia and Duarte, 2001). Such

514 easily utilizable organic matter, including dissolved monomeric carbohydrates, leaching out
515 during decomposition of *C. nodosa* leaves stimulated prokaryotic growth as previously
516 observed (Peduzzi and Herndl, 1991).

517 From July 2017 to March 2018, an adaptation of *C. nodosa* leaves to the decreasing light
518 and temperature occurred. Until October 2017, the temperature of the water column was still
519 optimal for elongation of the leaves and biomass increase, while the ambient light intensities
520 were continuously decreasing. An additional reduction of available light might occur from the
521 self-shading effect due to high canopy biomass, and/or shading due to epiphytic macroalgae
522 growth. Desaturation of low and fairly invariable lipids during the most active growth phase
523 suggested an increase in the membrane fluidity to optimize photosynthetic activity under low
524 light conditions. Such physiological adaptation was found in seagrasses living along a depth
525 gradient (Beca-Carretero et al., 2019) and macroalgae in contrasting seasons (Schmid et al.,
526 2014). In late autumn 2017 g 2018, the decrease in desaturation indicated a reduced fluidity
527 and activity of photosynthetically active membranes (Quigg et al., 2006; Wacker et al., 2016).
528 This was associated with a decreased abundance of shoots and above-ground biomass. By
529 shedding leaves and shoots the plant further balances metabolic requirements and mobilize
530 energy from the carbohydrate reserves stored in the below-ground tissue (Alcoverro et al.,
531 2001; Lee et al., 2007). During the winter, due to a sharp and continuous decrease in water
532 temperature, rapid desaturation of increasing lipids provided a cold resistance, as regularly
533 observed in algae and plants (Terrados and Lopezjimenez, 1996; Iveša et al., 2004; Upchurch,
534 2008).

535 In a healthy seagrass meadow, the oxygen generated by seagrass photosynthesis is
536 transported to below-ground tissues to maintain an oxic microsphere around roots and
537 rhizomes, re-oxidize sulfide to non-toxic S^0 , thus preventing an invasion of H_2S into the plant
538 (Pedersen et al., 1998; Holmer et al, 2005). S^0 was found in the *C. nodosa* below-ground
539 tissue during the entire investigation period, as already observed in seagrasses living in
540 sulfidic sediments (Holmer and Hasler-Sheetal, 2014; Hasler-Sheetal and Holmer, 2015). The
541 relatively low accumulation of H_2S ($< 30 \mu M$) during the summer and early autumn 2017
542 indicated that H_2S was apparently rapidly recycled within the rooted area via re-oxidation by
543 O_2 to S^0 and/or removal by precipitation with iron compounds. Most of S^0 was found in oxic
544 layers or suboxic/anoxic boundaries, being in ranges typical for sulfidic coastal sediments
545 (Troelsen and Jørgensen, 1982; Panutrakul et al., 2001; Pjevac et al., 2014). The oxidation of

546 H₂S could occur spontaneously by chemical reaction with free oxygen or mediated by sulfide-
547 oxidizing bacteria surrounding or being attached to seagrass roots (Jørgensen, 1977; Cucio et
548 al., 2016; Ugarelli et al., 2017; Fahimipour et al., 2017). In November, due to the degradation
549 of organic matter and reduced oxygen production and leakage in the rooted zone caused by *C.*
550 *nodosa* senescence, the re-oxidation capacity of the sediment was greatly decreased. This
551 resulted in considerable accumulation of H₂S (> 100 µM) which extended up to the sediment
552 surface. During winter and early spring, H₂S production generally decreased, likely due to the
553 reduced activity of sulfate reducing prokaryotes at lower temperatures, and the sediment
554 gradually shifted towards a more oxidized state. H₂S detected even in within the oxic
555 sediment and in the rooted area in February 2018 could be attributed to the sediment
556 heterogeneity and the presence of reducing micro-niches where anaerobic metabolism could
557 occur regardless of surrounding redox conditions (Jørgensen, 1977; Frederiksen and Glud,
558 2006).

559 In April 2018, *C. nodosa* had been most probably exposed to increased siltation, due to an
560 intensification of terrigenous input as indicated by a decrease in salinity (Δ 1.5 with respect to
561 March) and a substantial increase in particulate matter concentration (up to 3 times than in
562 March, Fig. 1b) combined with resuspension of sediment, provoking an elevated autotrophic
563 growth. The intensive siltation is associated with the increased light attenuation, both through
564 the direct shading effect of suspended sediments and through the promotion of phytoplankton
565 and epiphyte growth by the associated increase in nutrients (Terrados et al., 1998; Halun et
566 al., 2002; Brodersen et al., 2015). Therefore, the increase in seawater turbidity and
567 considerable sediment re-deposition on the leaves might have severely impaired the light
568 availability and slowed down the plant's photosynthetic activity as indicates LA/ALA > 1 in
569 the above-ground tissue resulting from decreased conversion of LA to ALA (Harris and
570 James, 1965). When the minimum light requirements (~14% of incidence light) are not met,
571 *C. nodosa* intensely sheds leaves and shoots (Collier et al., 2012). Such light condition
572 apparently persisted until May 2018 and most likely prevented the re-establishment of
573 photosynthesis and *C. nodosa* continued to shed shoots and leaves. The reduced
574 photosynthesis and therefore O₂ transport from the leaves to the rhizome-root system
575 probably minimized root respiration. The maintenance of the oxic rhizosphere and the internal
576 O₂ partial pressure in the lacunae further depended mainly on the diffusion of O₂ from the
577 water column. From April to June 2018, O₂ in the bottom water drastically decreased.

578 Although in such conditions of limited light and O₂ the seagrass might be capable for rapid
579 modulation of metabolic pathways and enhance its photosynthetic rate, as shown for *Zostera*
580 *muelleri* (Kim et al., 2018), it appeared that O₂ content of the *C. nodosa* below-ground tissue
581 was still too low to maintain the internal pressure and therefore, the plant tissues became
582 potentially accessible to sulfide intrusion (Pedersen et al., 2004).

583 At the same time, the sediment was enriched with fresh organic matter derived from
584 increased autotrophic biomass in bottom waters. In addition to the induction of the bloom,
585 strong sediment resuspension, most likely by aeration, stimulated the intense oxidation of H₂S
586 that started to produce in the rooted zone (up to 180 μM), due to increased activity of sulfate
587 reducing prokaryotes possibly triggered by the increase in temperature. An increase in S⁰
588 concentration that reached its maximum in the same layer suggests a simultaneous oxidation
589 of the produced H₂S. The sulfide oxidation probably caused oxygen depletion in the rooted
590 zone and anoxic zone extension up to the sediment subsurface. In May 2018, the excess of
591 organic matter accumulated in April 2018 was degraded. The concentrations of S⁰, detected
592 only in the suboxic layer, considerably decreased possibly by disproportionation or respiration
593 by members of the sulfate reducing bacteria (Pjevac et al., 2014).

594 During June and July 2018, a sudden and significant deterioration of *C. nodosa*
595 physiological condition was indicated by the further increase in LA/ALA ratio in the leaves
596 and overall saturation of decreasing lipids in above- and below-ground tissues. Additionally,
597 the loss of leaf tissue negatively impacted the photosynthetic carbon fixation and therefore
598 oxygen production, including the transport of oxygen to below-ground tissue (Lee and
599 Dunton, 1997; Lee et al., 2007). The below-ground tissue that was not supported by
600 photosynthetically derived oxygen became anoxic. Thus induced anaerobiosis most likely
601 caused a complete inhibition of the fatty acid desaturation chain (Harris and James, 1965) and
602 a permanent breakdown of photosynthesis leading to the final decay of the above-ground
603 biomass and considerable loss of below-ground biomass. As the bottom waters were
604 completely depleted in O₂ the whole plant was exposed to sulfides. H₂S inhibit cytochrome c
605 oxidase by binding to regulatory sites on the enzyme, reducing the rate of cellular respiration
606 and leading to the chemical asphyxiation (Nichols et al., 2013).

607 From June to August 2018, the decomposition of organic matter, encompassing the entire
608 sediment core, was intensified and accompanied by a large increase in H₂S concentrations (up
609 to 1200 μM). The degradation process involved rhizomes and roots, as suggested by the

610 apparent loss of below-ground biomass. Such loss typically occurs in the first stage of plant
611 decay, the leaching phase (Trevathan-Tackett et al., 2017). Readily available, soluble
612 carbohydrates that largely contribute to the leachate mass (Vichkovitten and Holmer, 2004)
613 most probably supported the increase in prokaryotic abundance observed in June and July
614 2018. However, the significant decrease in prokaryotic abundance that coincided with a
615 maximum degradation of organic matter and H₂S production in August 2018 might indicate
616 that remaining compounds were not degradable by the sulfate reduction pathway (Arndt et al.,
617 2013) and needed the presence of prokaryotes specialized in the anaerobic degradation of
618 refractory compounds, including cellulose and lignin.

619 During September and October 2018, H₂S concentrations drastically decreased, and the
620 sediment was gradually enriched in fresh organic matter. Due to the combined effect of
621 freshened oxygenated water inflow and resuspension which gradually deepened the oxic
622 layer, re-oxidation of H₂S increased. Biogeochemical studies suggest that most sulfides (80 –
623 90 %) are eventually re-oxidized; 10 – 20 % are ultimately buried as complexes with iron (i.e.
624 FeS, FeS₂) or with organic matter after sulfurization (Jørgensen, 1977; 1982). H₂S scavenging
625 with iron and formation of iron sulfides might be more important in Saline Bay, since
626 terrestrial waters are washing out *terra rossa*, rich in Fe-oxides and oxyhydroxides (Durn,
627 2003). For this reason, sediment cores were most likely always black with sulfuric odor,
628 irrespective of H₂S concentrations or presence of vegetation.

629

630 5 Conclusions

631 Our results provide insights into the interaction of multiple stressors that have led to the
632 meadow decay, triggered in the sensitive recruitment phase of meadow growth. Even after the
633 improvement of the sediment conditions by the end of the summer 2018, *C. nodosa* was not
634 able to recolonize its previously occupied areas. This finding combined with a visible
635 alteration of the water column and sediment indicates a considerable loss of the *C. nodosa*
636 habitat. Further research is needed to examine the fate of Saline Bay meadows and an
637 eventual recolonization of the area.

638 Beyond seagrass itself, this loss had extensive consequences as it has endangered many
639 species that depend on seagrass for food, shelter and nursery. Given the lack of data on the
640 ecological and conservation status of the still numerous seagrass meadows along the northern

641 Adriatic coast, the identification and monitoring of the main pressures acting on them are
642 needed to protect such valuable habitats from degradation and extinction.

643

644 *Author contribution:* Conceptualization: MN, MK and GJH; Investigation: MK, PP, MM, II,
645 LJI, IF and MN; Formal analysis and Writing - original draft: MN; Writing – review &
646 editing: MK, GJH, PP, LJI, II, IF and MM.

647 *Competing interests:* The authors declare that they have no conflict of interest.

648 *Acknowledgements.* The financial support was provided by the Croatian Science Foundation
649 to MN (project IP-2016-06-7118, MICRO-SEAGRASS). We sincerely thank J. Jakovčević
650 and M. Buterer for nutrient and chlorophyll *a* determination, and A. Budiša and I. Haberle for
651 occasional help during separation and biometry of plant material.

652

653 **References**

654 Agostini, S., Pergent, G., and Marchand, B.: Growth and primary production of *Cymodocea*
655 *nodosa* in a coastal lagoon. *Aquat. Bot.*, 76, 185-193, 2003.

656 Alcoverro, T., Manzanera, M., and Romero J.: Annual metabolic carbon balance of the
657 seagrass *Posidonia oceanica*: the importance of carbohydrate reserves. *Mar. Ecol. Prog.*
658 *Ser.*, 211, 105-116, 2001.

659 Arndt, S., Jørgensen, B.B., LaRowe, D.E., Middelburg, J.J., Pancost, R.D., and Regnier, P.:
660 Quantifying the degradation of organic matter in marine sediments: A review and
661 synthesis. *Earth-Science Rev.*, 123, 53-86, 2013.

662 Beca-Carretero, P., Guihéneuf, F., Marín-Guirao, L., Bernardeau-Esteller, J., García-Muñoz,
663 R., Stengel, D.B., and Ruiz, J.M. Effects of an experimental heat wave on fatty acid
664 composition in two Mediterranean seagrass species. *Mar. Pollut. Bull.*, 134, 27-37, 2018.

665 Beca-Carretero, P., Guihéneuf, F., Winters, G., and Stengel, D.B.: Depth-induced adjustment
666 of fatty acid and pigment composition suggests high biochemical plasticity in the tropical
667 seagrass *Halophila stipulacea*. *Mar. Ecol. Prog. Ser.*, 608, 105-117, 2019.

668 Borum, J., Pedersen, O., Greve, T.M. Frankovich, T.A., Zieman, J.C., Fourqurean, J.W., and
669 Madden, C.J.: The potential role of plant oxygen and sulphide dynamics in die-off events
670 of the tropical seagrass, *Thalassia testudinum*. *J. Ecol.*, 93, 148-158, 2005.

671 Bourbonniere, R.A., and Meyers, P.A.: Sedimentary geolipid records of historical changes in
672 the watersheds and productivities of Lakes Ontario and Erie. *Limnol. Oceanogr.*, 41, 352-
673 359, 1996.

674 Brodersen, K.E., Lichtenberg, M., Paz, L-C., and Kühl, M.: Epiphyte-cover on seagrass
675 (*Zostera marina* L.) leaves impedes plant performance and radial O₂ loss from the bellow-
676 ground tissue. *Front. Mar. Sci.*, 2, 58 doi: 10.3389/fmars.201500058, 2015.

677 Cancemi, G., Buia, M.C., and Mazzella, L.: Structure and growth dynamics of *Cymodocea*
678 *nodosa* meadows. *Sci. Mar.*, 66: 365-373, 2002.

679 Canfield, D.E., Jørgensen, B.B., Fossing, H., Glud, R., Gundersen, J., Ramsing, N.B.,
680 Thamdrup, B., Hansen, J.W., Nielsen, L.P., and Hall, P.O.J.: Pathways of organic carbon
681 oxidation in three continental margin sediments. *Mar. Geol.*, 113, 27-40, 1993.

682 Capone, D.G., and Kiene, R.P.: Comparison of microbial dynamics in marine and freshwater
683 sediments: Contrasts in anaerobic carbon catabolism. *Limnol. Oceanogr.*, 33, 725-749,
684 1988.

685 Carlson, P.R., Yarbrow, L.A., and Barber, T.R.: Relationship of sediment sulfide to mortality of
686 *Thalassia testudinum*, Florida Bay. *Bull. Mar. Sci.*, 54, 733-746, 1994.

687 Cebrian, J., Duarte, C.M., and Marbà, N.: Herbivory on the seagrass *Cymodocea nodosa*
688 (Ucria) Ascherson in contrasting Spanish Mediterranean habitats. *J. Exp. Mar. Biol. Ecol.*,
689 204, 103-111, 1996.

690 Cline, J.D.: Spectrophotometric determination of hydrogen sulfide in natural waters. *Limnol.*
691 *Oceanogr.*, 14, 454-458, 1969.

692 Collier, C.J., Lavery, P.S., Masini, R.J., and Ralph, P.J.: Shade-induced response and recovery
693 of the seagrass *Posidonia sinuosa*. *J. Exp. Mar. Biol. Ecol.*, 370, 89-103, 2009.

694 Collier, J.C., Waycott, M., and Giraldo Ospina, A.: Responses of four Indo-West Pacific
695 seagrass species to shading. *Mar. Pollut. Bull.*, 65, 342-354, 2012.

696 Costa, M.M., Barrote, I., Silva, J., Olivé, I., Alexandre, A., Albano, S., and Santos, R.:
697 Epiphytes modulate *Posidonia oceanica* photosynthetic production, energetic balance,
698 antioxidant mechanisms, and oxidative damage. *Front. Mar. Sci.* 2:111, 2015.

699 Cranwell, P.A., Eglinton, G., and Robinson, N.: Lipids of aquatic organisms as potential
700 contributors to lacustrine sediments. *Org. Geochem.*, 11, 513-527, 1987.

701 Cúcio, C., Engelen, A.H., Costa, R., and Muyzer, G.: Rhizosphere Microbiomes of European
702 Seagrasses Are Selected by the Plant, But Are Not Species Specific. *Front. Microbiol.*, 7,
703 440. doi: 10.3389/fmicb.2016.00440, 2012.

704 Duarte, C.M., Kennedy, H., Marbà, N., Gacia, E., Fourqurean, J.W., Beggins, J., Barrón, C.,
705 Apostolaki, E.T.: Seagrass community metabolism: Assessing the capacity of seagrass
706 meadows for carbon burial: Current limitations and future strategies. *Ocean Coast. Manag.*,
707 83, 32-38, 2013.

708 Durn, G.: *Terra Rossa* in the Mediterranean Region: Parent Materials, Composition and
709 Origin. *Geologia Croatica*, 56, 83-100, 2003.

710 Epstein, S.S., and Rossel J.: Enumeration of sandy sediment bacteria: search for optimal
711 protocol. *Mar. Ecol. Prog. Ser.*, 117, 289-298, 1995.

712 Fahimipour, A.K., Kardish, M.R., Lang, J.M., Green, J.L., Eisen, J.A., and Stachowicz, J.J.:
713 Global-Scale Structure of the Eelgrass Microbiome. *Appl. Environ. Microbiol.*, 83,
714 e03391-16, 2017.

715 Folk, R.L.: The distinction between grain size and mineral composition in sedimentary-rock
716 nomenclature. *J. Geol.*, 62, 344-359, 1954.

717 Frederiksen, M.S., Holmer, M., Pérez, M., Invers, O., Ruiz, J.M., and Knudsen, B.: Effect of
718 increased sediment sulfide concentrations on the composition of stable sulfur isotopes
719 ($\delta^{34}\text{S}$) and sulfur accumulation in the seagrasses *Zostera marina* and *Posidonia oceanica*.
720 *J. Exp. Mar. Biol. Ecol.*, 358, 98-109, 2008.

721 Frederiksen, M.S., and Glud, R.N.: Oxygen dynamics in the rhizosphere of *Zostera marina*: A
722 two-dimensional planar optode study. *Limnol. Oceanogr.*, 51, 1072-1083, 2006.

723 Gacia, E., and Duarte, C.M.: Sediment Retention by a Mediterranean *Posidonia oceanica*
724 Meadow: The Balance between Deposition and Resuspension. *Estuar. Coast. Shelf. Sci.*,
725 52, 505–514, 2001.

726 Gangi, A.F.: Permeability of unconsolidated sands and porous rocks. *J. Geophys. Res. –Solid*,
727 90, 3099-3104, 1985.

728 Gao, G., Clare, A.S., Chatzidimitriou, E., Rose, C., and Caldwell, G.: Effects of ocean
729 warming and acidification, combined with nutrient enrichment, on chemical composition
730 and functional properties of *Ulva rigida*. *Food Chem.*, 258, 71-78, 2018.

731 Greve, T.M., Borum, J., and Pedersen, O.: Meristematic oxygen variability in eelgrass
732 (*Zostera marina*). *Limnol. Oceanogr.*, 48, 210-216, 2003.

733 Halun, Z., Terrados, J., Borum, J., Kamp-Nielsen, J., Duarte, C.M., and Fortes, M.D.:
734 Experimental evaluation of the effects of siltation-derived changes in sediment conditions
735 on the Philippine seagrass *Cymodocea rotundata*. J. Exp. Mar. Biol. Ecol., 279, 73-87,
736 2002.

737 Harris, R.V., and James, A.T.: Linoleic and α -linolenic acid biosynthesis in plant leaves and a
738 green alga. Biochim. Biophys. Acta, 106, 456-464, 1965.

739 Hasler-Sheetal, H., and Holmer, M.: Sulfide intrusion and detoxification in the seagrass
740 *Zostera marina*. Plos One 10(6): e0129136, 2015.

741 Hendriks, I.E., Sintes, T., Bouma, T.J., and Duarte, C.M.: Experimental assessment and
742 modeling evaluation of the effects of the seagrass *Posidonia oceanica* on flow and particle
743 trapping. Mar. Ecol. Prog. Ser., 356, 163-173, 2008.

744 Holm-Hansen, O., Lorenzen, C. J., Holmes, R. W., and Strickland, J. D. H.: Fluorometric
745 determination of chlorophyll. J. Conseil., 301, 3-15, 1965.

746 Holmer, M., Duarte, C.M., Boschker, H.T.S., and Barrón, C.: Carbon cycling and bacterial
747 carbon sources in pristine and impacted Mediterranean seagrass sediments. Aquat. Microb.
748 Ecol., 36, 227-237, 2004.

749 Holmer, M., and Hasler-Sheetal, H.: Sulfide intrusion in seagrasses assessed by stable
750 isotopes- a synthesis of current results. Front. Mar. Sci., doi: 10.3389/fmars.2014.00064,
751 2014.

752 Holmer, M., and Nielsen, S.L.: Sediment sulfur dynamics related to biomass-density pattern
753 in *Zostera marina* (eelgrass) beds. Mar. Ecol. Prog. Ser., 146, 163-171, 1997.

754 Holmer, M., Frederiksen, M.S., and Møllegaard, H.: Sulfur accumulation in eelgrass (*Zostera*
755 *marina*) and effect of sulfur on eelgrass growth. Aquat. Bot., 81, 367-379, 2005.

756 Holmer, M., Pedersen, O., and Ikejima, K.: Sulfur cycling and sulfide intrusion in mixed
757 Southeast Asian tropical seagrass meadows. Bot. Mar., 49, 91-102, 2006.

758 Ivančić, I., Paliaga, P., Pfannkuchen, M., Đakovac, T., Najdek, M., Steiner, P., Korlević, M.,
759 Markovski, M., Baričević, A., Smodlaka Tanković, M., and Herndl, G.J.: Seasonal
760 variations in extracellular enzymatic activity in marine snow-associated microbial
761 communities and their impact on the surrounding water. FEMS Microbiol. Ecol., 94,
762 fyi198, 2018.

763 Iveša, Lj., Blažina, M., and Najdek, M.: Seasonal variations in fatty acid composition of
764 *Caulerpa taxifolia* (M. Vahl.) C. Ag. in the northern Adriatic Sea (Malinska, Croatia). Bot.
765 Mar., 47, 209-214, 2004.

766 Jørgensen, B.B.: The sulfur cycle of a coastal marine sediment (Limfjorden, Denmark).
767 Limnol. Oceanogr., 22, 814-832, 1977.

768 Jørgensen, B.B.: Mineralization of organic matter in the sea bed - the role of sulphate
769 reduction. Nature, 296, 643-645, 1982.

770 [Kim, M., Brodersen, K.E., Szabó, M., Larkum, A.W.D., Raven J.A., Ralph, P.J., and Pernice,](#)
771 [M.: Low oxygen affects photophysiology and the level of expression of two-carbon](#)
772 [metabolism genes in the seagrass *Zostera muelleri*. Photosynth. Res., 136, 147-160, 2018.](#)

773 Koch, M.S., and Erskine, J.M.: Sulfide as a Phytotoxin to the Tropical Seagrass *Thalassia*
774 *testudinum*: Interactions with Light, Salinity and Temperature. J. Exp. Mar. Biol. Ecol.,
775 266, 81-95, 2001.

776 Krause-Jensen, D., Carstensen, J., Nielsen, S.L., Dalsgaard, T., Christensen, P.B., Fossing, H.,
777 and Rasmussen, M.B.: Sea bottom characteristics affect depth limits of eelgrass *Zostera*
778 *marina*. Mar. Ecol. Prog. Ser., 425, 91-102, 2011.

779 Lee, K-S., and Dunton, K.H.: Diurnal changes in pore water sulfide concentrations in the
780 seagrass *Thalassia testudinum* beds: the effects of seagrasses on sulfide dynamics. J. Exp.
781 Mar. Biol. Ecol., 255, 201-214, 2000.

782 Lee, K-S., Park, S.R., and Kim, Y.K.: Effects of irradiance, temperature, and nutrients on
783 growth dynamics of seagrasses: A review. J. Exp. Mar. Biol. Ecol., 350, 144-175, 2007.

784 Marbà, N., and Duarte, C.M.: Growth and sediment space occupation by seagrass *Cymodocea*
785 *nodosa* roots. Mar. Ecol. Prog. Ser., 224, 291-298, 2001.

786 Mascaró, O., Valdemarsen, T., Holmer, M., Pérez, M., and Romero, J.: Experimental
787 manipulation of sediment organic content and water column aeration reduces *Zostera*
788 *marina* (eelgrass) growth and survival. J. Exp. Mar. Biol. Ecol., 373, 26-34, 2009.

789 Micromeritics: SediGraph 5100 particle size analysis system operator' manual. Micromeritics
790 Instrument Corporation, Norcross, 2002.

791 Moeslund, L., Thamdrup, B., and Jørgensen, B.B.: Sulfur and iron cycling in a coastal
792 sediment—radiotracer studies and seasonal dynamics. Biogeochemistry, 27, 129-152,
793 1994.

794 Nicholls, P., Marshall, D.C., Cooper, C.E., and Wilson, M.T.: Sulfide inhibition of and
795 metabolism by cytochrome c oxidase. *Biochem. Soc. Transact.*, 41, 1312-1316, 2013.

796 Orlando-Bonaca, M., Francé, J., Mavrič, B., Grego, M., Lipej, L., Flander Putrle, V., Šiško,
797 M., and Falace, A.: A new index (MediSkew) for the assessment of the *Cymodocea nodosa*
798 (Ucria) Ascherson meadow's status. *Mar. Environ. Res.*, 110, 132-141, 2015.

799 Orlando-Bonaca, M., Francé, J., Mavrič, B., and Lipej, L.: Impact of the Port of Koper on
800 *Cymodocea nodosa* meadow. *Annales*, 29, 187-194, 2019.

801 Orth, R.J., Carruthers, T.J.B., Dennison, W.C., Duarte, C.M., Fourqurean, J.W., Heck Jr.,
802 K.L., Hughes, A.R., Kendrick, G.A., Kenworthy, E.J., Olyarnik, S., Short, F.T., Waycott,
803 M., and Williams, S.L.: A Global Crisis for Seagrass Ecosystems. *BioScience*, 56, 987-
804 996, 2006.

805 Panutrakul, S., Monteny, F., and Baeyens, W.: Seasonal Variations in Sediment Sulfur
806 Cycling in the Ballastplaat Mudflat, Belgium. *Estuaries* 24, 257-265, 2001.

807 Pedersen, M.F., Duarte, C.M., and Cebrián, J.: Rates of changes in organic matter and nutrient
808 stocks during seagrass *Cymodocea nodosa* colonization and stand development. *Mar. Ecol.*
809 *Prog. Ser.*, 159, 29-36, 1997.

810 Pedersen, O., Borum, J., Duarte, C.M., and Fortes, M.D.: Oxygen dynamics in the rhizosphere
811 of *Cymodocea rotundata*. *Mar. Ecol. Prog. Ser.*, 169, 283-288, 1988.

812 Pedersen, O., Binzer, T., and Borum, J.: Sulphide intrusion in eelgrass (*Zostera marina* L.).
813 *Plant Cell Environ.*, 27, 595-602, 2004.

814 Peduzzi, P., and Herndl, G.J.: Decomposition and significance of seagrass litter (*Cymodocea*
815 *nodosa*) for the microbial food web in coastal waters (Gulf of Trieste, Northern Adriatic
816 Sea). *Mar. Ecol. Prog. Ser.*, 71, 163-174, 1991.

817 Pérez, M., Invers, O., Ruiz Fernandez, J.M., Frederiksen, M., and Holmer, M.: Physiological
818 responses of the seagrass *Posidonia oceanica* to elevated organic matter content in
819 sediments: An experimental assessment. *J. Exp. Mar. Biol. Ecol.*, 344, 149-160, 2007.

820 Pirini, M., Manuzzi, M.P., Pagliarani, A., Trombetti, F., Borgatti, A.R., and Ventrella, V.:
821 Changes in fatty acid composition of *Mytilus galloprovincialis* (Lmk) fed on microalgal
822 and wheat germ diets. *Comp. Biochem. Physiol. B*, 147, 616-626, 2007.

823 Pjevac, P., Kamyshny Jr., A., Dyksma, S., and Mussmann, M.: Microbial consumption of
824 zero-valence sulfur in marine benthic habitats. *Environ. Microbiol.*, 16, 3416-3430, 2014.

825 Porter, K.G., and Feig, Y.S.: The use of DAPI for identification and counting aquatic
826 microflora. *Limnol. Oceanogr.*, 25, 943-984, 1980.

827 Quigg, A., Kevekordes, K., Raven, J., and Beardall, J.: Limitations on microalgal growth at
828 very low photon fluency rates: the role of energy slippage. *Photosynth. Res.*, 88, 299-310,
829 2006.

830 Rogowska, J., Sychowska, J., Cieszynska-Semenowicz, M., and Wolska, L.: Elemental sulfur
831 in sediments: analytical problems. *Environ. Sci. Pollut. Res.*, 23, 24871-24879, 2016.

832 Samper-Villarreal, J., Lovelock, C.E., Saunders, M.I., Roelfsema, C., and Mumby, P.J.:
833 Organic carbon in seagrass sediment is influenced by seagrass canopy complexity,
834 turbidity, wave height, and water depth. *Limnol. Oceanogr.*, 61, 938-952, 2016.

835 Sand-Jensen, K., Pedersen, O., Binzer, T., and Borum, J.: Contrasting Oxygen Dynamics in
836 the Freshwater Isoetid *Lobelia dortmanna* and the Marine Seagrass *Zostera marina*. *Ann.*
837 *Bot.*, 96, 613-623, 2005.

838 Schmid, M., Guihéneuf, F., and Stengel, D.B.: Fatty acid contents and profiles of 16
839 macroalgae collected from the Irish Coast at two seasons. *J. Appl. Phycol.*, 26, 451-463,
840 2014.

841 Short, F.T., Polidoro, B., Livingstone, S.R., Carpenter, K.E., Bandeira, S., Bujang, J.S.,
842 Calumpong, H.P., Carruthers, T.J.B., Coles, R.G., Dennison, W.C., Erftemeijer, P.L.A.,
843 Fortes, M.D., Freeman, A.S., Jagtap, T.G., Kamal, A.M., Kendrick, G.A., Kenworthy,
844 W.J., La Nafie, Y.A., Nasution, I.M., Orth, R.J., Prathep, A., Sanciangco, J.C., van
845 Tussenbroek, B., and Vergara, S.G.: Extinction risk assessment of the world's seagrass
846 species. *Biol. Conserv.*, 144, 1961-1971, 2011.

847 Sousa, A.I., Calado, R., Cleary, D.F.R., Nunes, C., Coimbra, M.A., Serôdio, J., and Lillebø,
848 A.I.: Effect of spatio-temporal shifts in salinity combined with other environmental
849 variables on the ecological processes provided by *Zostera noltii* meadows. *Sci. Rep.*, 7,
850 1336, 2017.

851 Strickland, J.D.H., and Parsons, T.R.: A practical handbook of seawater analysis. *Bull. Fish.*
852 *Res. Board. Can.*, 167,1-310, 1972.

853 Terrados, J., and Lopez-Jimenez, J.A.: Fatty acid composition and chilling resistance in the
854 green alga *Caulerpa prolifera* (Forsskal) Lamouroux (Chlorophyta, Caulerpales). *Biochem.*
855 *Molecul. Biol. Internatl.*, 39, 863-869, 1996.

856 Terrados, J., Duarte, C.M., Fortes, M.D., Borum, J., Agawin, N.S.R., Bach, S., Thampanya,
857 U., Kamp-Nielsen, L., Kenworthy, W.J., Geertz-Hansen, O., and Vermaat, J.: Changes in
858 Community Structure and Biomass of Seagrass Communities along Gradients of Siltation
859 in SE Asia. *Estuar. Coast. Shelf Sci.*, 46, 757-768, 1998.

860 Terrados, J., and Ros, J.D.: Growth and primary production of *Cymodocea nodosa* (Ucria)
861 Ascherson in a Mediterranean coastal lagoon: the Mar Menor (SE Spain). *Aquat. Bot.*, 43,
862 63-74, 1992.

863 Trevathan-Tackett, S.M., Seymour, J.R., Nielsen, D.A., Macreadie, P.I., Jeffries, T.C.,
864 Sanderman, J., Baldock, J., Howes, J.M., Steven, A.D.L., and Ralph, P.J.: Sediment anoxia
865 limits microbial-driven seagrass carbon remineralization under warming conditions. *FEMS*
866 *Microbiol. Ecol.*, 93,fix033, 2017.

867 Troelsen, H., and Jørgensen, B.B.: Seasonal dynamics of elemental sulfur in two coastal
868 sediments. *Estuar. Coast. Shelf Sci.*, 15, 255-266, 1982.

869 Tuya, F., Martín, J.A., and Luque, A.: Impact of a marina construction on seagrass bed at
870 Lanzarote (Canary Islands). *J. Coast. Conserv.*, 8, 157-162, 2002.

871 Tuya, F., Ribeiro-Leite, L., Arto-Cuesta, N., Coca, J., Haroun, R., and Espino, F.: Decadal
872 changes in the structure of *Cymodocea nodosa* seagrass meadows: Natural vs. human
873 influences. *Estuar. Coast. Shelf Sci.*, 137, 41-49 (2014).

874 Ugarelli, K., Chakrabarti, S., Laas, P., and Stingl, U.: The seagrass holobiont and its
875 microbiome. *Microorganisms* 5, 81, 2017.

876 Upchurch, R.G.: Fatty acid unsaturation, mobilization, and regulation in the response of plants
877 to stress. *Biotechnol. Lett.*, 30, 967-977, 2008.

878 Valentine, J.F., and Duffy, J.E.: The central role of grazing in seagrass ecology. In:
879 *Seagrasses: Biology, Ecology and Conservation*, Springer, Netherlands, pp 431-501, 2006.

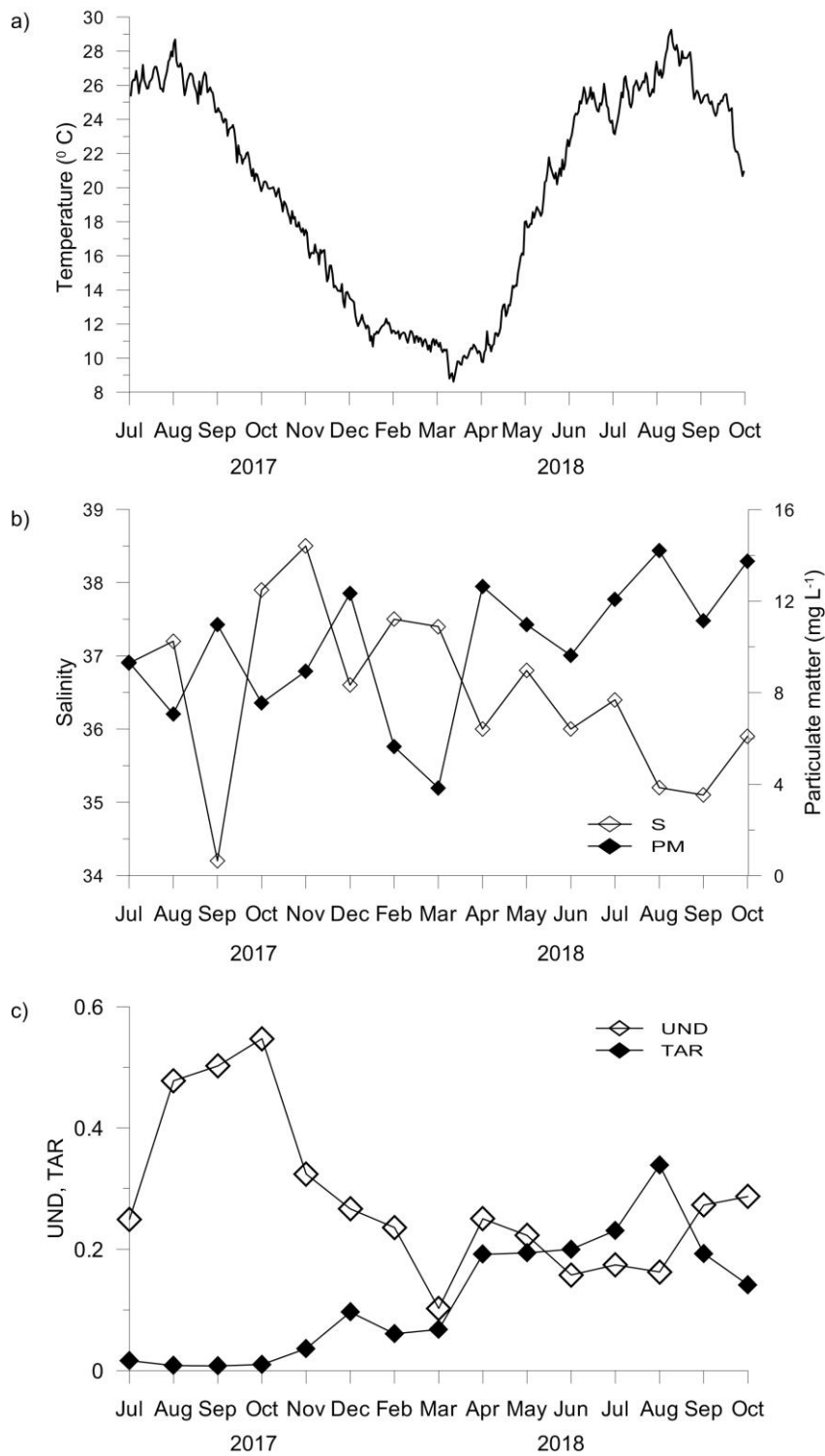
880 Vaquer-Sunyer, R., and Duarte, C.M.: Thresholds of hypoxia for marine biodiversity. *PNAS*,
881 105, 15452-15457, 2008.

882 Vaquer-Sunyer, R., and Duarte, C.M.: Sulfide exposure accelerates hypoxia-driven mortality.
883 *Limnol. Oceanogr.*, 55, 1075-1082, 2010.

884 Viso, A.C., Pesando, D., Bernard, P., and Marty, J.C.: Lipid components of the Mediterranean
885 seagrass *Posidonia oceanica*. *Mar. Pollut. Bull.*, 34, 381-387, 1993.

886 Vichkovitten, T., and Holmer, M.: Contribution of plant carbohydrates to sedimentary carbon
887 mineralization. *Org. Geochem.*, 35,1053-1066, 2004.

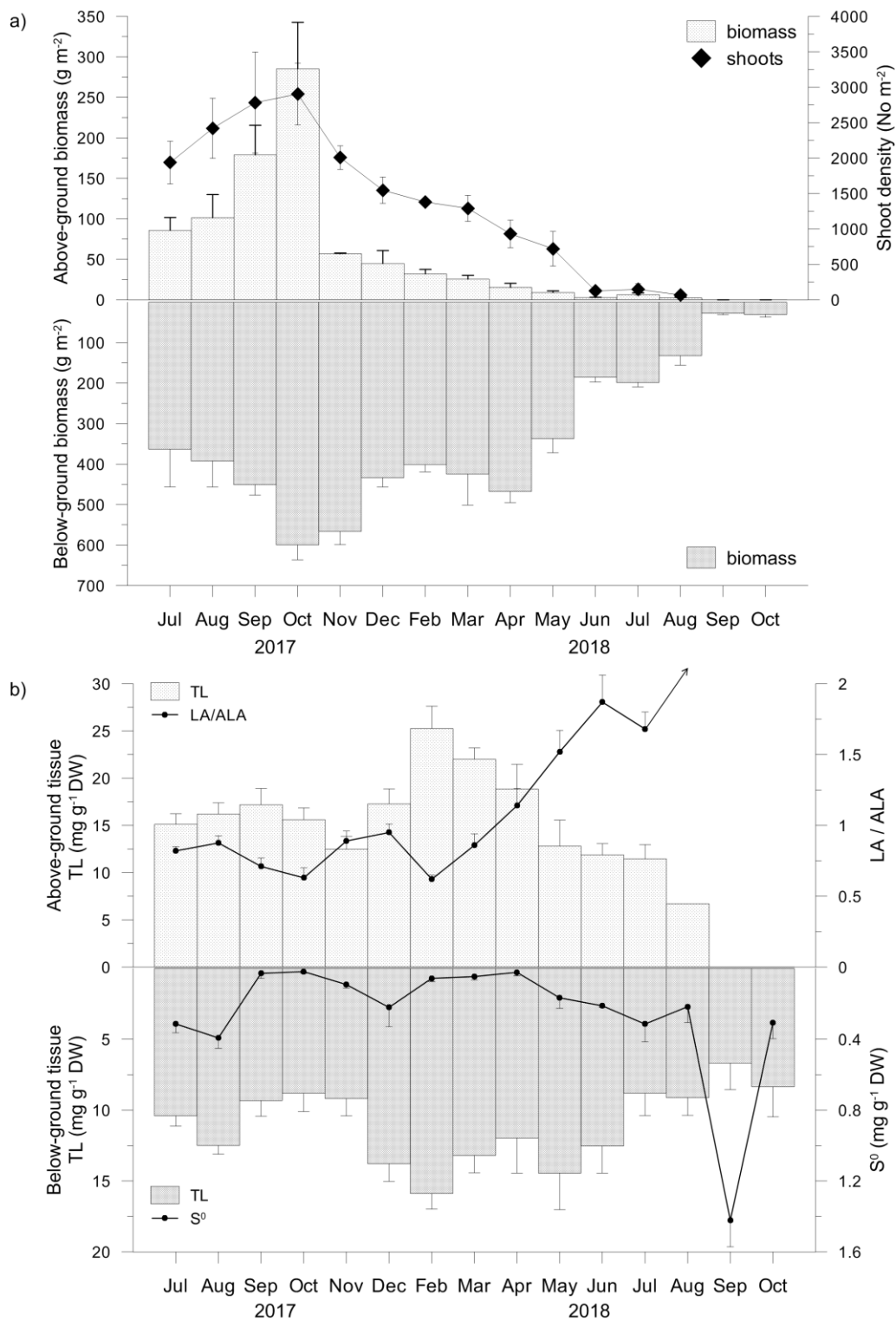
- 888 Wacker, A., Piepho, M., Harwood, J.L., Guschina, I.A., and Arts, M.T.: Light-induced
889 changes in fatty acid profiles of specific lipid classes in several freshwater phytoplankton
890 species. *Front. Plant Sci.*, 7, 264, 2016.
- 891 Widdows, J., Pope, N.D., Brinsley, M.D., Asmus, H., and Asmus, R.M.: Effects of seagrass
892 beds (*Zostera noltii* and *Z. marina*) on near-bed hydrodynamics and sediment
893 resuspension. *Mar. Ecol. Prog. Ser.*, 358, 125-136, 2008.
- 894 Zavodnik, N., Travizi, A., and De Rosa, S.: Seasonal variations in the rate of photosynthetic
895 activity and chemical composition of the seagrass *Cymodocea nodosa* (Ucr.) Asch. *Sci.*
896 *Mar.*, 62, 301-309, 1998.



897

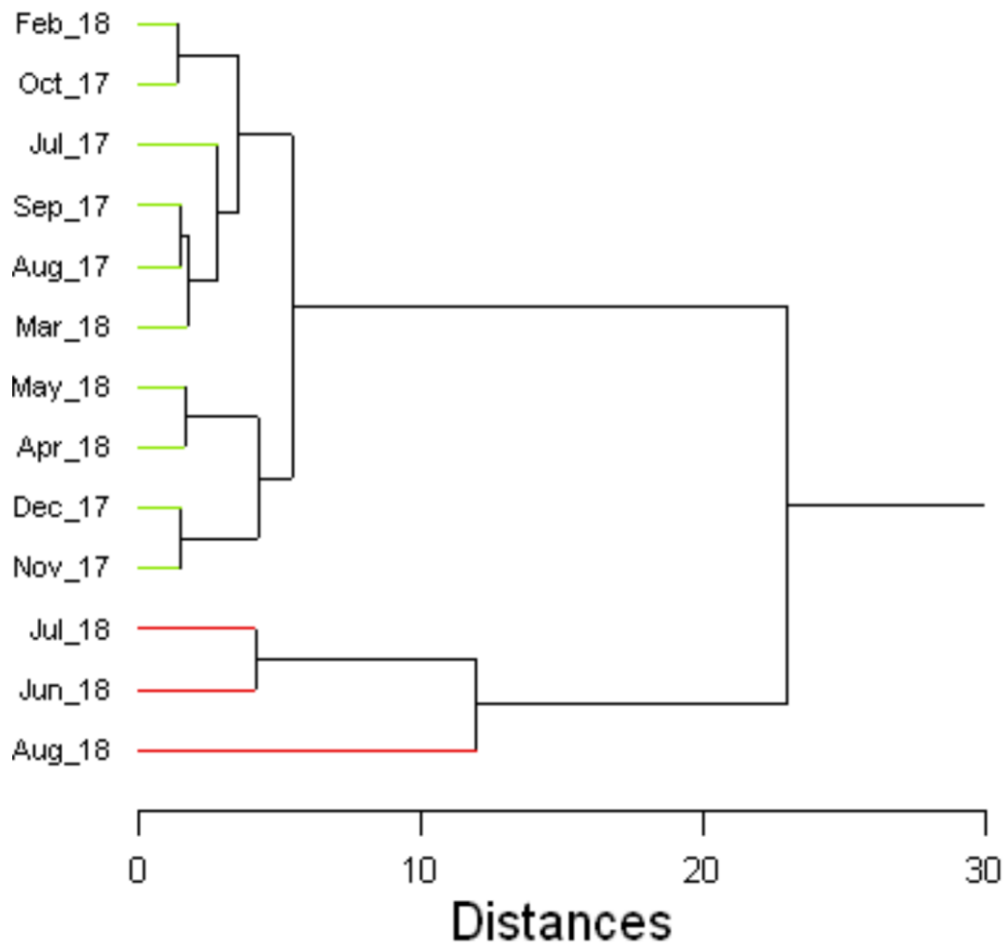
898

899 Figure 1. Temperature (a); salinity (b), particulate matter concentration (b); unsaturation
 900 degree (UND) and terrestrial to aquatic ratio (TAR) of the particulate lipid matter (c) in
 901 seawater.



902

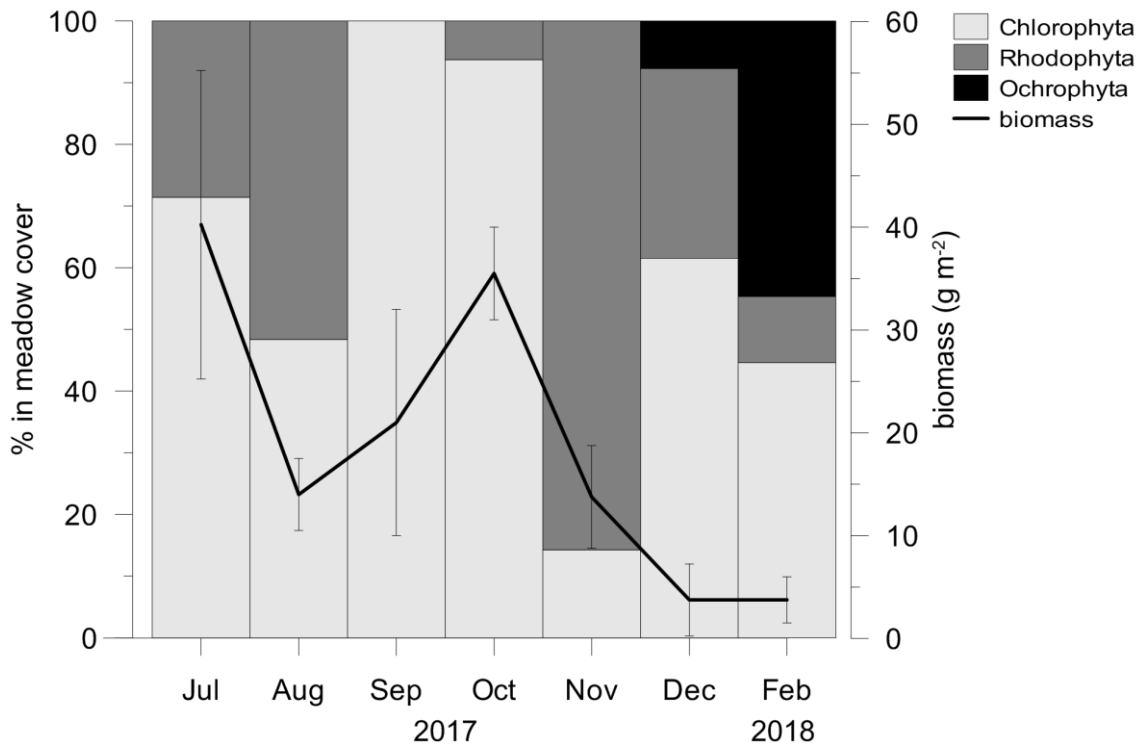
903 Figure 2. Above- and below-ground tissue biomasses and shoot density (a), total lipid
 904 concentrations (TL) and linoleic to α -linolenic fatty acids ratios (LA/ALA, an arrow indicates
 905 an infinite value) in above-ground tissue and TL and approximated concentrations of
 906 elemental sulfur (S⁰) in below-ground tissue (b).



907

908 Figure 3. Cluster analysis dendrogram of fatty acid composition of *C. nodosa* leaves.

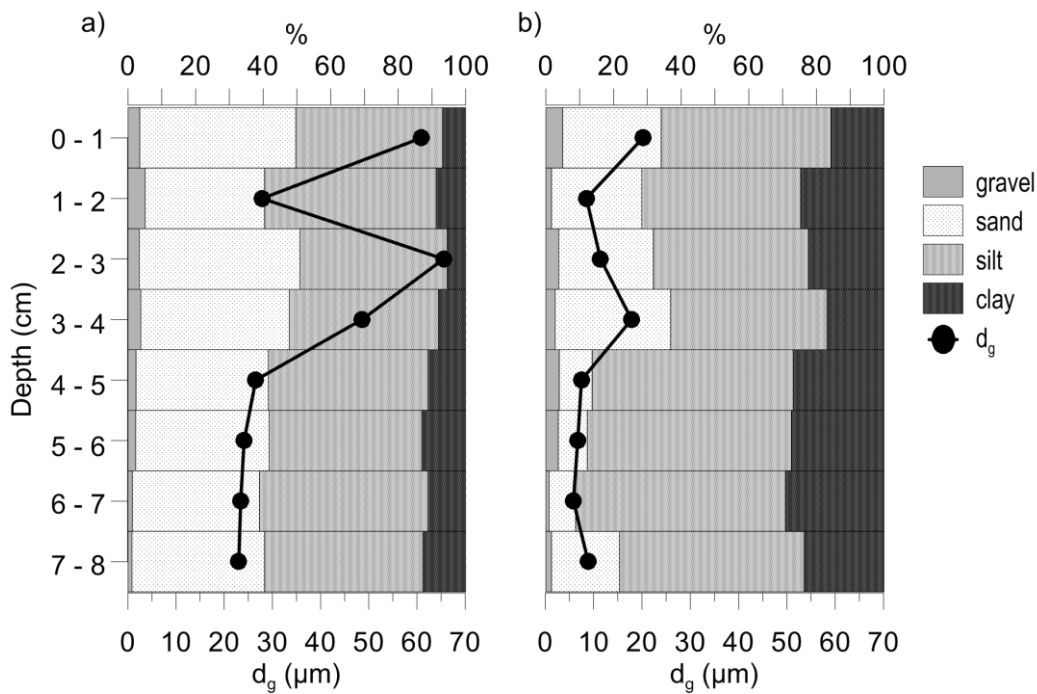
909 Summary statistics is given in Table S3.



910

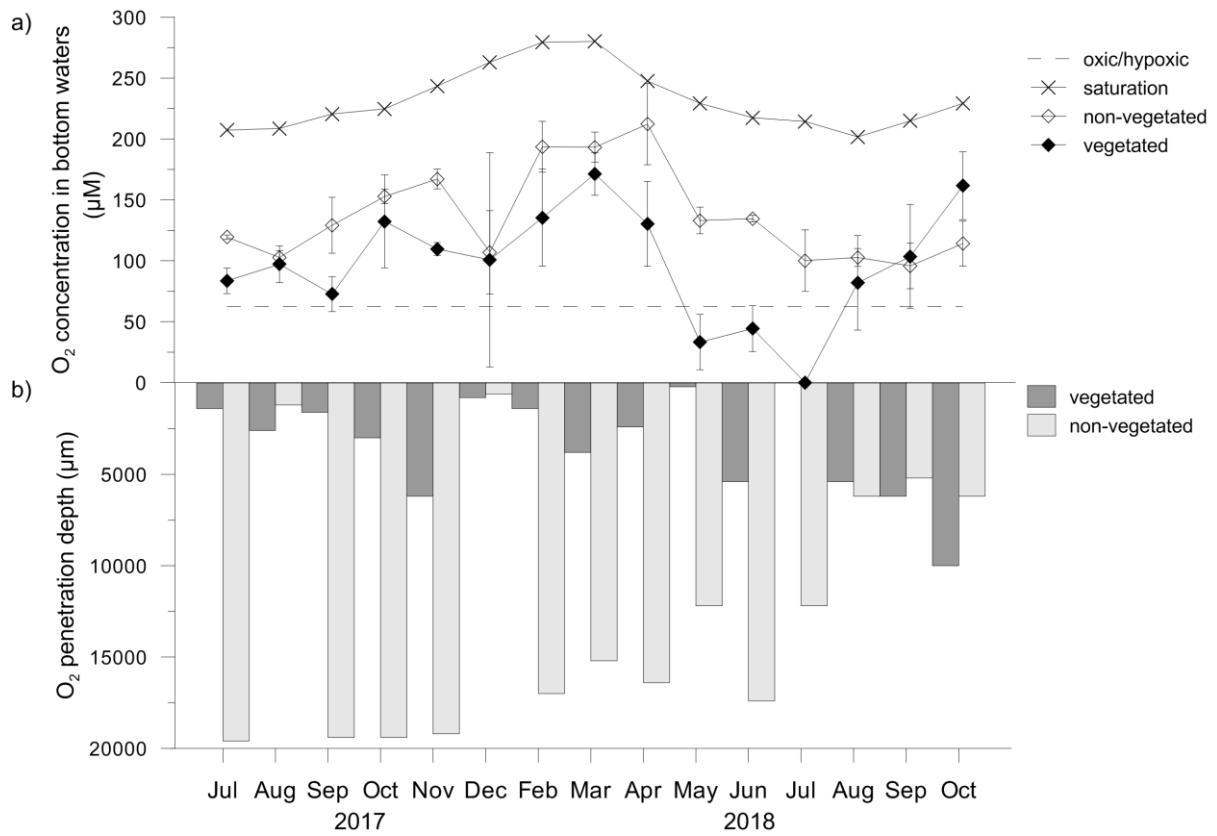
911 Figure 4. The contribution of macroalgal phyla in a meadow cover and total macroalgal
 912 biomass. After February 2018 macroalgae were no longer present in the *C. nodosa* meadow.

913



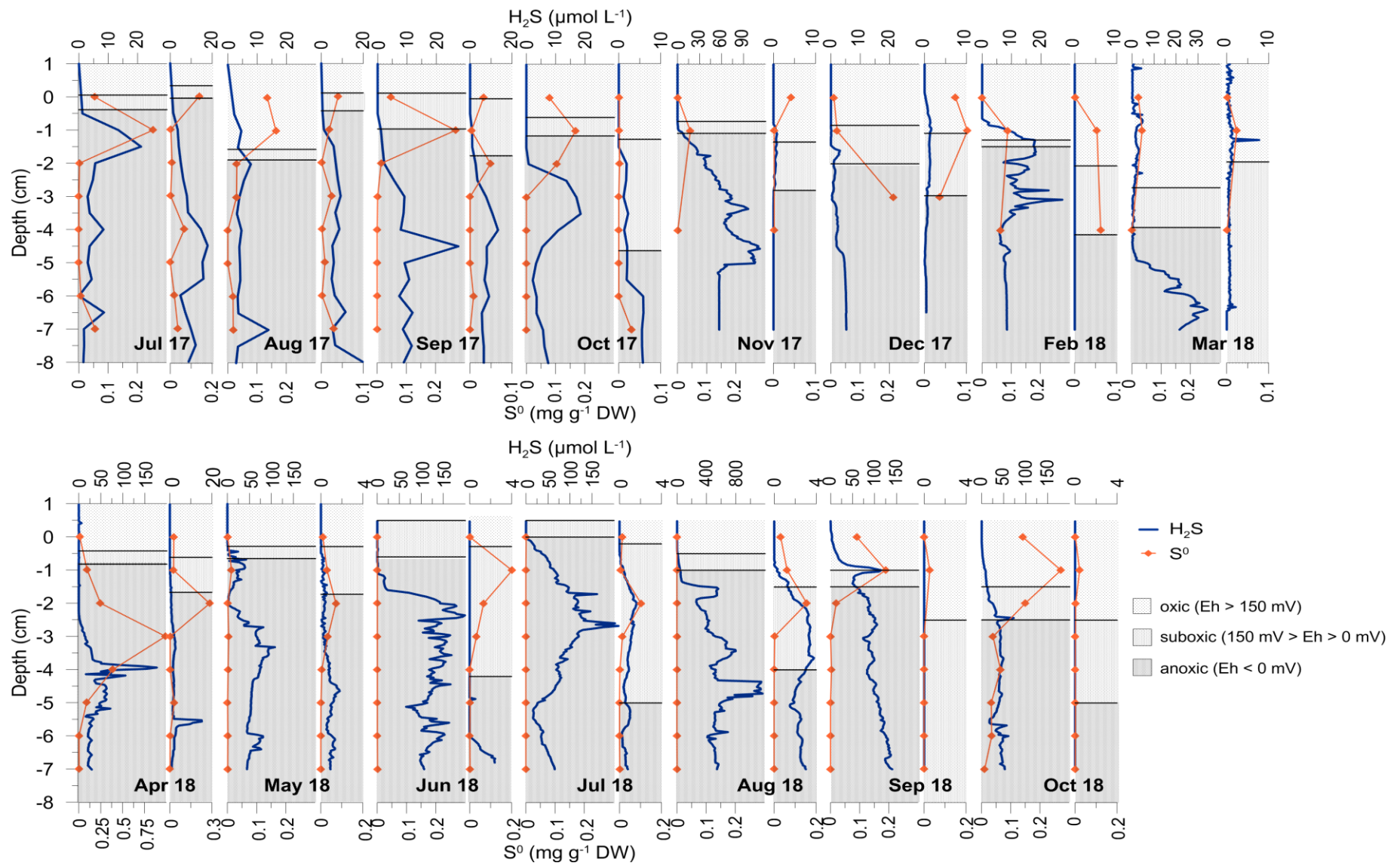
914

915 Figure 5. Granulometric composition and median grain size (d_g) of vegetated (a) and non-
 916 vegetated sediment (b).



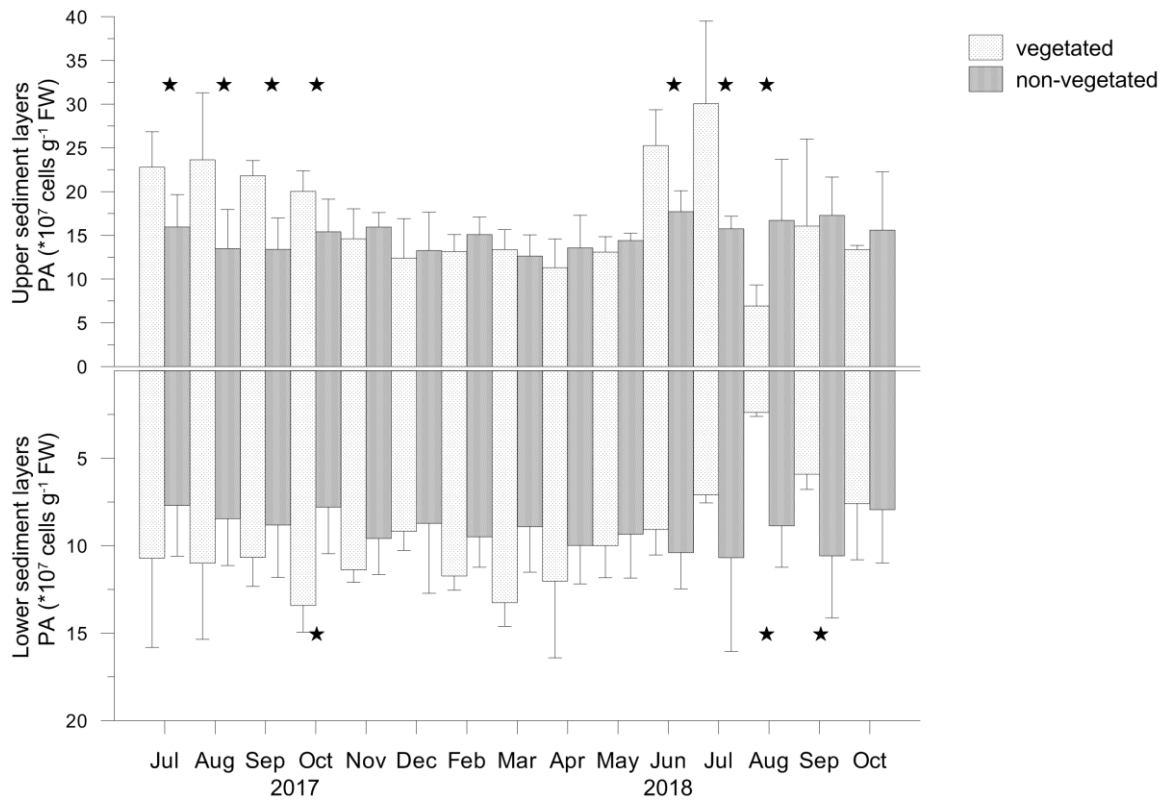
917

918 Figure 6. Oxygen concentrations (O₂) in bottom waters (a) and O₂ penetration depths (b)
 919 above and in vegetated and non-vegetated sediment, respectively. O₂ at the saturation level
 920 was calculated according to the temperature and salinity measured in seawater at the sampling
 921 dates; O₂ at the hypoxic frontier (~ 62.5 µM) was taken from Vaquer-Sanyer and Duarte
 922 (2008).



923

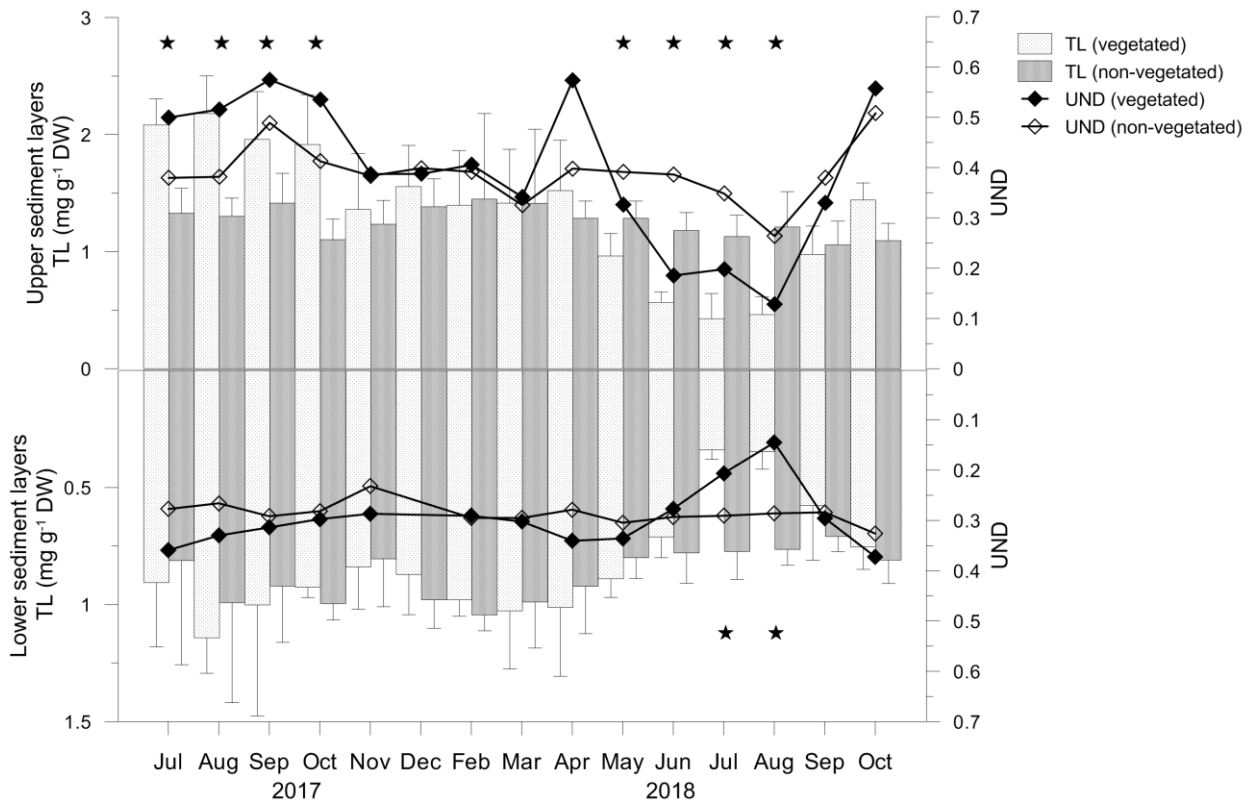
924 Figure 7. Depth profiles of H_2S and S^0 concentrations in vegetated and non-vegetated sediment (adjacent narrow graphs). The redox potential
 925 (Eh) in both sediments is shown as areas corresponding to oxic ($\text{Eh} > 150 \text{ mV}$), suboxic ($150 > \text{Eh} > 0 \text{ mV}$) and anoxic ($\text{Eh} < 0 \text{ mV}$) conditions.



926

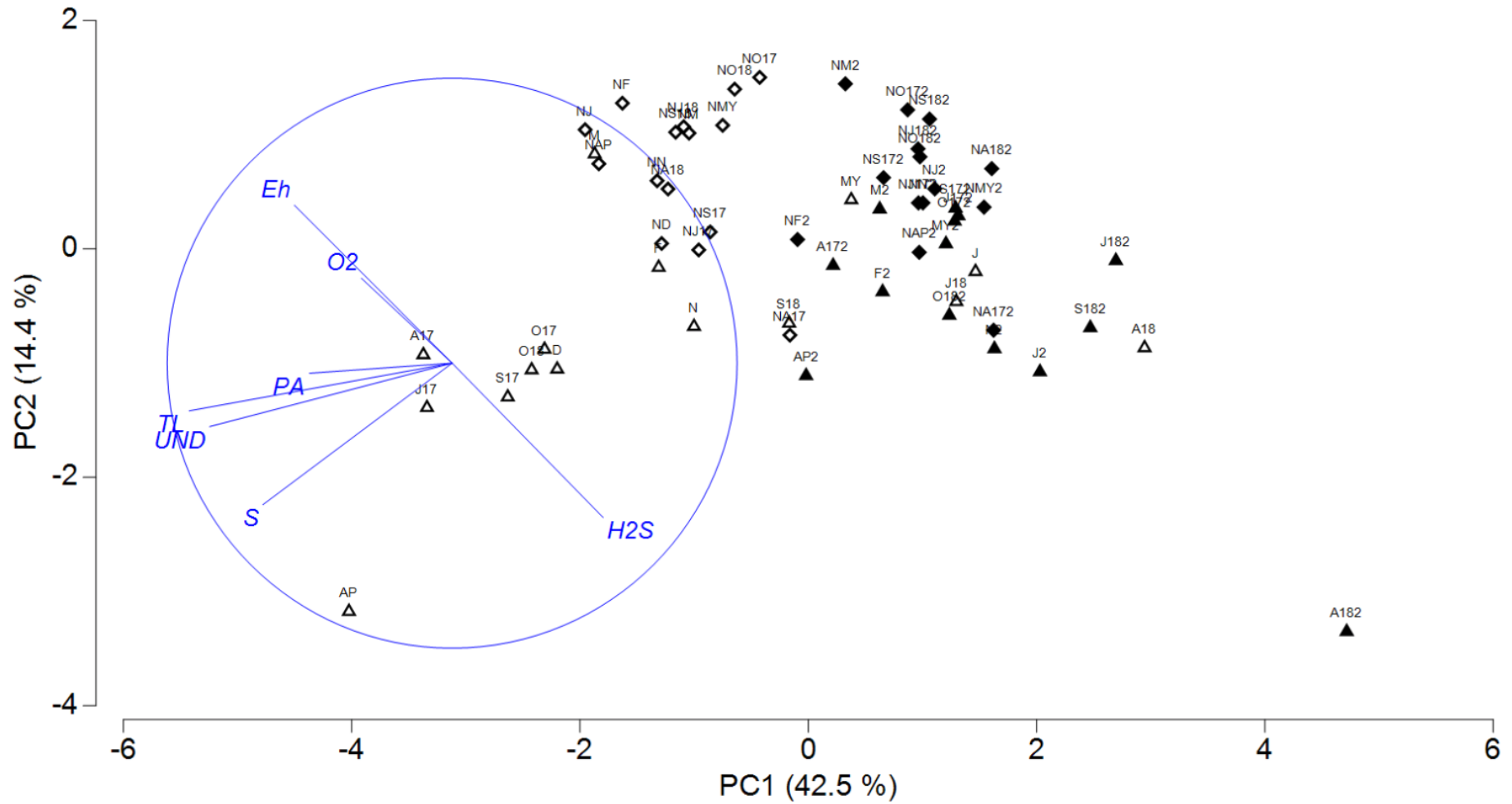
927 Figure 8. Prokaryotic abundance (PA) in the upper (0 - 4 cm) and lower (5 - 8 cm) layers of
 928 vegetated and non-vegetated sediments; significant differences in PA between the sediments
 929 are indicated by asterisks.

930



931

932 Figure 9. Total lipid concentrations (TL) and unsaturation degree (UND) in the upper (0 - 4
 933 cm) and lower (5 - 8 cm) layers of vegetated and non-vegetated sediments. Significant
 934 differences in TL between the sediments are indicated by asterisks.



936

937 Figure 10. PCA plot of redox potential (Eh), oxygen (O₂), hydrogen sulfide (H₂S), sulfur (S), total lipids (TL) and prokaryotes (PA)
 938 concentrations and unsaturation degree (UND) in the upper (0 – 4 cm; △, ◇) and lower (5 – 7 cm; ▲, ◆) layers of vegetated and non-vegetated
 939 sediments, respectively. Projections of variables are given in circle